1   **TITLE**

2   **Lysine63-linked ubiquitin chains earmark GPCRs for BBSome-**

3   **mediated removal from cilia**

4   **AUTHORS:** Swapnil Rohidas Shinde, Andrew R. Nager[#] and Maxence V. Nachury[*]

5   **AFFILIATION:**

6   Department of Ophthalmology, University of California San Francisco, CA 94143, USA

7

8   *   Correspondence: maxence.nachury@ucsf.edu

9   #   Current address: Cancer Immunology Discovery, Pfizer Inc., San Diego, CA, 92121, USA

ABSTRACT (158 words)

Regulated trafficking of G-protein coupled receptors (GPCRs) controls cilium-based signaling pathways. β-arrestin, a molecular sensor of activated GPCRs, and the BBSome, a complex of Bardet-Biedl Syndrome (BBS) proteins, are required for the signal-dependent exit of ciliary GPCRs but the functional interplay between β-arrestin and the BBSome remains elusive. Here we find that, upon activation, ciliary GPCRs become tagged with K63-linked ubiquitin (K63Ub) chains in a β-arrestin-dependent manner prior to BBSome-mediated exit. Removal of ubiquitin acceptor residues from the somatostatin receptor 3 (SSTR3) and from the orphan GPCR GPR161 demonstrates that ubiquitination of ciliary GPCRs is required for their regulated exit from cilia. Furthermore, targeting a K63Ub-specific deubiquitinase to cilia blocks the exit of GPR161, SSTR3 and Smoothened (SMO) from cilia. Finally, ubiquitinated proteins accumulate in cilia of mammalian photoreceptors and *Chlamydomonas* cells when BBSome function is compromised. We conclude that K63Ub chains mark GPCRs and other unwanted ciliary proteins for recognition by the ciliary exit machinery.

INTRODUCTION

The regulated trafficking of signaling receptors in and out of cilia is a central regulatory mechanism of many cilia-based signaling pathways (Nachury and Mick, 2019; Anvarian et al., 2019; Mykytyn and Askwith, 2017; Gigante and Caspary, 2020). For example, upon activation of the Hedgehog signaling pathway, the Hedgehog receptor Patched 1 and the G protein-coupled receptor (GPCR) GPR161 disappear from cilia while GPCR Smoothened (SMO) accumulates in cilia (Rohatgi et al., 2007; Corbit et al., 2005; Mukhopadhyay et al., 2013). In all three cases, regulated exit from cilia plays a major role in the on-demand redistribution of signaling molecules (Nachury and Mick, 2019). Signal-dependent exit is likely to be a general characteristic of ciliary GPCRs as the Somatostatin Receptor 3 (SSTR3), the Dopamine Receptor 1 (D1R), the Melanocortin concentrating hormone receptor 1 (MCHR1) and the neuropeptide receptor 2 (NPY2R) all disappear from cilia upon exposure to agonist (Domire et al., 2011; Loktev and Jackson, 2013; Nager et al., 2017; Green et al., 2015). A major question is how GPCRs are selected for removal from cilia in an activity-dependent manner.

The major trafficking entities mediating signal-dependent exit from cilia are the BBSome and β-arrestin 2. The BBSome is an evolutionarily conserved complex of eight Bardet-Biedl Syndrome (BBS) proteins that directly recognizes intracellular determinants in GPCRs and ferries them out of cilia (Nachury, 2018; Wingfield et al., 2018). The BBSome associates with the intraflagellar transport (IFT) machinery and has been proposed to act as adaptor between the motor-driven intraflagellar transport trains and the membrane proteins that are to be removed from cilia. Because the BBSome is not known to have the ability to discriminate active from inactive GPCRs, there must exist another layer of regulation that commits activated GPCRs for exit. β-arrestin 2 is a well-established molecular sensor of the activation state of GPCRs that is required for the signal-dependent exit of GPR161 and SSTR3 (Pal et al., 2016; Green et al., 2015; Nager et al., 2017). No association of β-arrestin 2 with ciliary trafficking complexes has been reported to date and it remains unclear how β-arrestin 2 relays information regarding the state of activation of ciliary GPCRs to the ciliary exit machinery.

53 An emerging player in ciliary exit is ubiquitination (Shearer and Saunders, 2016). Ubiquitin (Ub),

54 a 76-amino acid polypeptide, becomes conjugated to acceptor lysine residues on substrate

55 proteins by ubiquitin ligases and tags substrates for degradation or other regulatory fates (Yau

56 and Rape, 2016; Swatek and Komander, 2016). A role for ubiquitin in promoting ciliary exit is

57 suggested by multiple lines of evidence. First, interfering with Patched1 ubiquitination blocks its

58 signal-dependent exit from cilia (Kim et al., 2015; Yue et al., 2014). Second, fusing ubiquitin to

59 PKD-2, the olfactory receptor ODR-10 or the TRP channel OSM-9 at their cytoplasmic end

60 results in the disappearance of these proteins from cilia (Hu et al., 2007; Xu et al., 2015). The

61 accumulation of these ubiquitin fusions inside cilia when BBSome function is compromised

62 suggests that the BBSome might sort ubiquitinated signaling receptors out of cilia, in line with a

63 reported association of BBSome with ubiquitinated proteins in trypanosomes (Langousis et al.,

64 2016). Interestingly, TRIM32 is a ubiquitin ligase mutated in BBS patients (Chiang et al., 2006).

65 Third, the ubiquitin ligase Cbl is recruited to cilia upon activation of the ciliary tyrosine kinase

66 receptor PDGFRαα and Cbl is required for termination of PDGFRαα signaling (Schmid et al.,

67 2018). Last, a dramatic rise in ubiquitination of the ciliary proteome is observed when

68 *Chlamydomonas* cilia disassemble (Huang et al., 2009). In particular, α-tubulin becomes

69 ubiquitinated on K304 upon cilia disassembly and expression of α-tubulin[K304R] slows down

70 cilia disassembly (Wang et al., 2019).

71 After conjugation onto substrates, ubiquitin itself often serves as a substrate for ubiquitination.

72 The resulting ubiquitin chains are characterized by the acceptor lysine residue on ubiquitin with

73 lysine 48-linked Ub (UbK48) chains targeting soluble proteins for proteasomal degradation while

74 lysine 63-linked Ub (UbK63) chains assembled onto membrane proteins constitute the major

75 driver for sorting from the limiting membrane of late endosomes into intralumenal vesicles and

76 ultimately lysosomal degradation (Piper et al., 2014; Yau and Rape, 2016; Swatek and

77 Komander, 2016). Intriguingly, in shortening *Chlamydomonas* cilia K63Ub linkages predominate

78 at least 5-fold over K48 linkages and only K63Ub linkages are detected on α-tubulin. A role for

79 K63Ub chains in ciliary trafficking remains to be determined.

4

80   Together, these data led us to investigate the interplay between ubiquitination, β-arrestin 2 and

81   the ciliary exit machinery. Using a combination of cellular imaging, biochemical studies and

82   cilia-specific manipulations, we find that β-arrestin 2 directs the activation-dependent addition of

83   K63-linked ubiquitin chains onto ciliary GPCRs that are then selected by the BBSome for

84   removal from cilia.

85 **RESULTS**

86 **Signal-dependent ubiquitination of ciliary GPCRs is required for their regulated**

87 **exit from cilia**

88 As a first step in investigating the interplay between ubiquitination and the ciliary exit machinery,

89 we sought to determine whether activation of ciliary GPCRs leads to their ubiquitination inside

90 cilia prior to retrieval into the cell. We blocked BBSome-dependent exit by deleting its cognate

91 GTPase ARL6/BBS3 in mouse inner medulla collecting duct (IMCD3) cells. IMCD3 cells

92 represent a validated cell culture system to study ciliary trafficking and the IMCD3 $Arl6^{-/-}$ line has

93 been previously characterized (Liew et al., 2014; Ye et al., 2018). As in previous studies (Ye et al.,

94 2018; Nager et al., 2017), all GPCRs were expressed at near-endogenous levels by driving

95 expression with extremely weak promoters. The fluorescent protein mNeonGreen (NG) fused to

96 the cytoplasm-facing C-terminus of GPCRs allowed direct visualization. A biotinylation

97 Acceptor Peptide (AP) fused to the extracellular N-terminus biotinylated by an ER-localized

98 biotin ligase (BirA-ER) enabled pulse labeling of surface-exposed molecules and denaturing

99 purifications. When SSTR3 was expressed in $Arl6^{-/-}$ IMCD3 cells, addition of its agonist

100 somatostatin (sst) led to a drastic increase in the ciliary levels of ubiquitin observed upon

101 immunostaining with the well-characterized FK2 (**Figure 1A-B)** and FK1 (**Figure S1A-B**)

102 monoclonal antibodies (Fujimuro et al., 1994; Emmerich and Cohen, 2015; Haglund et al.,

103 2003). All further experiments were conducted with the FK2 antibody. $Arl6^{-/-}$ cells accumulated

104 Ub signals inside cilia in the absence of SSTR3 expression (**Figure 1A-B**), demonstrating that

105 some endogenous proteins become ubiquitinated inside the cilia of $Arl6^{-/-}$ IMCD3 cells. No

106 ubiquitin signal was detected inside cilia when BBSome function was intact (**Figure 1A-B and**

107 **S1A-D**), indicating that the BBSome efficiently removes ubiquitinated proteins from cilia.

108 Because the sst-dependent increase in ciliary ubiquitin signal depends upon SSTR3 expression

109 (**Figure 1A-B**), these results suggest that either SSTR3 itself or a downstream effector of SSTR3

110 become ubiquitinated inside cilia upon activation.

111   To determine whether SSTR3 becomes ubiquitinated in response to sst, we biochemically

112   isolated ^{AP}SSTR3^{NG} under denaturing conditions via the biotinylated AP tag and probed for

113   ubiquitin via an HA tag on transfected HA-Ub. As typical for a glycosylated protein, SSTR3

114   migrated as a broad band centered around 100 kDa (**Figure 1C**). The amount of SSTR3

115   recovered did not change appreciably between WT and *Arl6$^{-/-}$* cells or upon stimulation with sst

116   (**Figure 1C**). Remarkably, while only very faint Ub signals were detected associated with SSTR3

117   in WT cells, a Ub smear extending from 100 kDa upward was detected in the SSTR3 pull-downs

118   from *Arl6$^{-/-}$* cells. Furthermore, stimulation with sst resulted in a modest but reproducible

119   increase in SSTR3 ubiquitination in *Arl6$^{-/-}$* cells (**Figure 1D**). We conclude that the

120   BBSome/ARL6 system is required for the degradation of ubiquitinated SSTR3 and that SSTR3

121   becomes ubiquitinated in response to stimulation with sst.

122   We next sought to test whether signaling receptors endogenous to IMCD3 cells are ubiquitinated

123   inside cilia in an activity-dependent manner. One signaling pathway that is natively expressed in

124   IMCD3 cells is the Hedgehog pathway. Prior experiments have detected normal trafficking

125   dynamics of SMO and GPR161 in IMCD3 cells (Ye et al., 2018; Mukhopadhyay et al., 2013)

126   and **Figure 4D**). As GPR161 and SMO both accumulate in cilia of *Arl6$^{-/-}$* cells without Hh

127   pathway stimulation (Liew et al., 2014; Zhang et al., 2011), the ubiquitin signal detected in *Arl6$^{-/-}$*

128   cilia may correspond to ubiquitin conjugated to SMO or GPR161. We detected a significant

129   elevation of the ciliary ubiquitin levels in *Arl6$^{-/-}$* cells when treated with the SMO agonist SAG

130   (**Figure 1E-F**). Because SMO ubiquitination was previously shown to decrease upon its

131   activation (Xia et al., 2012; Jiang et al., 2019), it is likely that the elevated ciliary ubiquitin signal

132   detected in SAG-treated cells is associated with GPR161. As activation of SMO triggers exit of

133   GPR161 but this exit is frustrated when BBSome function goes awry, these data suggest that

134   GPR161 becomes ubiquitinated prior to its BBSome-dependent exit. Collectively, these data

135   suggest that GPCRs are ubiquitinated in a regulated fashion inside cilia and subsequently

136   retrieved into the cell by the BBSome.

137   To test the functional importance of GPCR ubiquitination in BBSome-mediated exit from cilia,

138   we removed all ubiquitination sites from SSTR3 and GPR161 by mutating all cytoplasm-

7

139   exposed lysine residues to arginine (cK0 variants). Exit kinetics were precisely monitored by real-

140   time tracking of individual cilia in live cells. In both cases, the cK0 variant underwent markedly

141   slower signal-dependent exit from cilia than the WT allele (**Figure 2A-B**). Measurement of exit

142   rates revealed that exit of SSTR3cK0 was ~2-fold slower than SSTR3 and that exit of

143   GPR161cK0 was ~2.5-fold slower than GPR161. The residual exit rates of the cK0 mutants

144   indicate the existence of alternative mechanisms of exit that complement GPCR ubiquitination

145   or bypass BBSome-dependent retrieval (see discussion).

146   To rule out that the observed ciliary exit defect of the cK0 mutants was an indirect consequence

147   of defective endocytosis for example because of clogging of the ciliary exit path, we directly

148   assessed endocytosis of SSTR3 and SSTR3cK0. The surface-exposed pool of [AP]SSTR3 was pulse

149   labeled with fluorescently labeled monovalent streptavidin (mSA) and cells were stimulated with

150   sst. The faint hazy signal corresponding to the plasma membrane pool of SSTR3 disappeared

151   after 10 min in the presence of sst in a similar fashion for both WT and cK0 variants (**Figure

152   2C**). Concurrently, the WT and cK0 variants appeared in cytoplasmic foci corresponding to

153   endocytic vesicles (**Figure 2C**). Counting cytoplasmic foci revealed that endocytosis proceeded

154   normally irrespective of the ubiquitination competence of SSTR3 (**Figure 2D**). SSTR3 thus

155   behaves similarly to nearly every GPCR tested to date, in that it does not require ubiquitination

156   for its signal-dependent internalization. Indeed, while ubiquitination of plasma membrane

157   proteins is a major driver of internalization in yeast, ubiquitination of signaling receptors is

158   generally dispensable for signal-dependent internalization in mammalian cells (Dores and Trejo,

159   2019; Piper et al., 2014; Skieterska et al., 2017).

160   These results strongly support a direct role for GPCR ubiquitination in promoting signal-

161   dependent exit from cilia.

162

163   **Ciliary K63 ubiquitin linkages are required for GPCR exit**

164   We next sought to characterize the type of ubiquitin conjugates that are attached to ciliary

165   proteins. The FK1 and FK2 antibodies used in our immunofluorescent studies recognize

8

166   ubiquitin either as single adduct or in chain but not free ubiquitin (Fujimuro et al., 1994;

167   Emmerich and Cohen, 2015). The availability of antibodies specific for K48 and K63 ubiquitin

168   linkages (Newton et al., 2008) enabled us to determine the types of ubiquitin conjugates that are

169   attached to ciliary GPCRs. While we found no detectable signal for K48-linked ubiquitin chains

170   (UbK48) in cilia, the signal for K63-linked ubiquitin (UbK63) linkages mirrored the ciliary

171   response observed with the FK1 and FK2 antibody in IMCD3-[SSTR3] cells subjected to

172   agonist treatment (**Figure 3A-B and S1C-D**). Given the high specificity and selectivity of the

173   K48 and K63 linkage antibodies, these data strongly suggest that K63Ub chains are added onto

174   SSTR3 inside cilia upon activation.

175   To confirm that K63 of Ub is the main linkage used for the elongation of Ub chains on SSTR3,

176   we transfected variants of ubiquitin with lysines mutated to arginines into $Arl6^{-/-}$ cells stably

177   expressing SSTR3. Signal-dependent ubiquitination of SSTR3 was abrogated when all seven

178   lysines of Ub were mutated to arginines (**Figure 3C-D**). However, when K63 was the only lysine

179   left intact on Ub, signal-dependent ubiquitination of SSTR3 was restored to the same extent as

180   with WT Ub (**Figure 3C-D**). We conclude that UbK63 chains are assembled onto SSTR3 in

181   response to SSTR3 activation inside cilia.

182   To determine the functional importance of UbK63 linkages in tagging GPCRs for exit from cilia,

183   we sought to specifically interfere with UbK63 linkages inside cilia (**Figure 4A**). Structural and

184   biochemical studies have demonstrated that the deubiquitinase AMSH possesses a near-absolute

185   specificity for UbK63 linkages and does not cleave other Ub chain linkages or Ub-substrates

186   linkages (Sato et al., 2008; McCullough et al., 2004). AMSH normally function on the surface of

187   late endosomes in concert with the endosomal sorting complex required for transport (ESCRT)

188   protein STAM (McCullough et al., 2006). AMSH was previously fused to the epidermal growth

189   factor receptor EGFR to demonstrate that UbK63 chains assembled on EGFR are dispensable

190   for internalization but required for sorting into lysosomes (Huang et al., 2013). We targeted

191   AMSH to cilia using the well-validated ciliary targeting signal from the ciliopathy protein

192   NPHP3 (Nakata et al., 2012; Wright et al., 2011) and analyzed the exit of three distinct GPCRs:

193   SMO, GPR161 and SSTR3. To alleviate concerns related to the interaction of AMSH with the

194   STAM, we deleted the STAM-interacting domain of AMSH and only expressed the catalytic

195   domain of AMSH. The signal-dependent exit of SSTR3 was assessed by treating IMCD3-

196   [SSTR3] cells with sst for 2h. In cells expressing cilia-AMSH (a fusion of NPHP3[1-200] to GFP

197   and the catalytic domain of AMSH), sst no longer triggered a significant reduction in the ciliary

198   levels of SSTR3 (**Figure 4B-C**). Care was taken to only analyze cells that expressed modest

199   levels of cilia-AMSH as judged by GFP fluorescence (**Figure S3**). In contrast, SSTR3 exit

200   proceeded normally in cells that expressed NPHP3[1-200]-GFP alone or a catalytically dead

201   variant of cilia-AMSH that we named cilia-ASMH[†] (**Figure 4B-C**). These controls strongly

202   suggest that cilia-AMSH exerts its effects on SSTR3 exit by cleaving UbK63 chains inside cilia, a

203   conclusion borne out by imaging ciliary UbK63 in cells transfected with cilia-AMSH (**Figure**

204   **S4**). Similarly, the exit of endogenous GPR161 from RPE cell cilia upon activation of the

205   Hedgehog pathway was abolished in cells expressing moderate levels of cilia-AMSH (**Figure**

206   **4D-E**). Neither NPHP3[1-200]-GFP nor cilia-AMSH[†] blocked the signal-dependent exit of

207   GPR161 from cilia (**Figure 4D-E**).

208   Unlike GPR161 and other ciliary GPCRs such as the Somatostatin receptor 3 (SSTR3) that are

209   removed from cilia by the BBSome only when they become activated, SMO undergoes

210   constitutive BBSome-dependent exit from cilia in the absence of Hedgehog pathway stimulation

211   (Nachury, 2018; Ye et al., 2018; Ocbina and Anderson, 2008; Zhang et al., 2011). Signal-

212   dependent accumulation of SMO in cilia is achieved, at least in part, by suppression of its exit

213   (Milenkovic et al., 2015; Nachury and Mick, 2019; Ye et al., 2018). In cells expressing cilia-

214   AMSH, endogenous SMO spontaneously accumulated inside cilia in the absence of Hedgehog

215   pathway activation (**Figure 4F-G**). Again, neither NPHP3[1-200]-GFP nor cilia-AMSH[†]

216   influenced the ciliary accumulation of SMO (**Figure 4F-G**).

217   Together, these results indicate that K63-linked ubiquitin chains inside cilia, presumably built

218   onto each ciliary GPCRs under a specific signaling stimulus, are required for GPCR removal

219   from cilia.

220

10

β-arrestin 2 mediates signal-dependent ubiquitination of ciliary GPCRs

As β-arrestin 2 is required for signal-dependent exit of GPR161 and SSTR3 from cilia (Green et al., 2015; Pal et al., 2016; Ye et al., 2018), we sought to determine the functional relationship between β-arrestin 2 and the BBSome. As previously described (Green et al., 2015), β-arrestin 2 is initially undetectable inside cilia and becomes recruited to cilia within minutes of SSTR3 agonist addition (**Figure 5A-C**). The ciliary β-arrestin 2 signal reaches a plateau after about 10 min and the $t_{1/2}$ for ciliary accumulation is less than 5 min (**Figure 5C**). Meanwhile the $t_{1/2}$ for BBSome recruitment to the tip of cilia was 10 min and the first signs of detectable SSTR3 exit were seen between 10 and 15 min (**Figure 5C**). These kinetics suggested that β-arrestin 2 is first recruited to activated ciliary SSTR3 before the BBSome ferries activated SSTR3 out of cilia. When ARL6 was depleted, the basal levels of ciliary β-arrestin 2 were elevated but the kinetics of β-arrestin 2 accumulation in cilia upon SSTR3 activation were indistinguishable from control-depleted cells (**Figure 5A-B**). These data suggest that a small fraction of SSTR3 that is tonically active fails to exit cilia in ARL6-depleted cells and recruits β-arrestin 2. From these data, we conclude that β-arrestin 2 functions either upstream of, or in parallel with the BBSome in signal-dependent retrieval of GPCRs. Similarly, the kinetics of GPR161 exit and β-arrestin 2 ciliary recruitment upon activation of the Hh pathway indicated that β-arrestin 2 reaches its maximal ciliary level before the first signs of GPR161 exit become evident (**Figure 5D**).

We previously proposed that β-arrestin 2 may bridge activated GPCRs to the BBSome (Ye et al., 2018; Nachury, 2018). Yet, we have thus far failed to detect a biochemical interaction between β-arrestin 2 and the BBSome. Furthermore, the continuous distribution patterns of β-arrestin 2 and SSTR3 inside cilia are similar to one another and distinct from the discontinuous pattern of the BBSome (**Figure 5A**), arguing against a direct association of β-arrestin 2 with BBSome/IFT trains inside cilia. We considered the alternative hypothesis that β-arrestin 2 function upstream of the BBSome. Given that β-arrestin 2 functions in the signal-dependent targeting of GPCRs from the plasma membrane to the lysosome by recruiting ubiquitin ligases to activated GPCRs (Henry et al., 2012; Bhandari et al., 2007; Shenoy et al., 2008; Martin et al., 2003), we posited that β-arrestin 2 recognizes activated GPCRs inside cilia to direct their ubiquitination and subsequent

11

249   selection by the BBSome for removal from cilia. A central prediction of this model is that β-

250   arrestin 2 is required for the ubiquitination of ciliary GPCRs in response to stimulation. To test

251   this prediction, we deleted the β-arrestin 2 gene *Arrb2* in *Arl6* knockout IMCD3 cells (Nager et

252   al., 2017). While the signal-dependent exit of SSTR3 from cilia failed in both *Arl6⁻ᐟ⁻* and *Arl6⁻ᐟ⁻*

253   *Arrb2⁻ᐟ⁻* cells (**Figures 1A-B and 6A-B**), ubiquitin staining in cilia and by inference signal-

254   dependent ubiquitination of SSTR3 was only observed in *Arl6⁻ᐟ⁻* cells (**Figures 6A-B**). In *Arl6⁻ᐟ⁻*

255   *Arrb2⁻ᐟ⁻* cells, the signal-dependent increase in ciliary ubiquitin signal was no longer observed

256   (**Figures 6A-B**). Similarly, the increase in ciliary ubiquitin signal seen in *Arl6⁻ᐟ⁻* cells treated with

257   the Hedgehog pathway agonist SAG was no longer observed in the absence of β-arrestin 2

258   (**Figure 6C-D**). These data indicate that, in the absence of BBSome function, ciliary GPCRs

259   become ubiquitinated in response to activation in a β-arrestin 2-dependent manner. We sought

260   to confirm our imaging-based finding with a biochemical analysis of SSTR3 ubiquitination.

261   While SSTR3 ubiquitination was readily detected in *Arl6⁻ᐟ⁻* cells and measurably increased upon

262   stimulation with sst, the deletion of β-arrestin 2 in *Arl6⁻ᐟ⁻* cells drastically reduced SSTR3

263   ubiquitination levels and no sst-dependent increase of SSTR3 ubiquitination was detected in

264   *Arl6⁻ᐟ⁻ /Arrb2⁻ᐟ⁻* cells (**Figure 6E-F**).

265   Together, these data suggest the following order of action: GPCR activation, β-arrestin 2

266   engagement, Ub ligase recruitment, assembly of K63Ub chains on the GPCR, and finally

267   selection of ubiquitinated GPCRs for BBSome-mediated retrieval (**Figure 7E**).

268

269   **Constitutively retrieved BBSome cargoes are ubiquitinated prior to exit**

270   Besides removing GPCRs from cilia in a regulated fashion, the BBSome also clears cilia of

271   unwanted proteins that accidentally enter cilia. In the single-cell flagellated organism

272   *Chlamydomonas reinhardtii*, mutations in the BBSome subunit Bbs4 cause a constitutive

273   accumulation of several proteins including Phospholipase D in cilia (Lechtreck et al., 2009).

274   When stained for ubiquitin, *Bbs4 Chlamydomonas* showed a 2-fold enrichment in ciliary signal

275   compared to WT (**Fig. 7A-B**). Isolation of cilia revealed the accumulation of ubiquitin

276   conjugates above 80 kDa in *Bbs4* mutant *Chlamydomonas* cilia (**Fig. 7C**). These results are

277   consistent with the hypothesis that ciliary proteins subject to constitutive retrieval are

278   ubiquitinated prior to their removal from cilia by the BBSome.

279   In the mammalian retina, proteomics studies have found over 100 proteins accumulating in the

280   outer segment (the equivalent of the cilium) of *Bbs* photoreceptors compared to WT

281   photoreceptors (Datta et al., 2015). When we stained sections of mouse retina for ubiquitin, we

282   found a drastic accumulation of ubiquitin signal in the outer segment of $Bbs4^{-/-}$ photoreceptors

283   compared to WT photoreceptors (**Fig. 7D**). We note that the nature of ubiquitin conjugates

284   remains to be determined in the case of constitutive cargoes. These results suggest that a variety

285   of proteins that accidentally flow into the photoreceptors outer segments –possibly caught on the

286   tremendous flux of rhodopsin trafficking to the outer segment (Baker et al., 2008)– are recognized

287   as foreign to the cilium, ubiquitinated on site and selected for removal by the BBSome (**Figure**

288   **7E**).

289   **DISCUSSION**

290   **Recognition of K63-linked ubiquitin chains by the ciliary exit machinery**

291   Our results indicate that K63-linked ubiquitin chains tag activated GPCRs and likely other

292   unwanted proteins for BBSome-mediated removal from cilia. Prior findings in trypanosomes

293   suggest that the BBSome may directly recognize ubiquitin (Langousis et al., 2016), although

294   direct biochemical evidence and information regarding ubiquitin chain specificity is still missing.

295   It is also known that the BBSome directly recognizes cytoplasmic determinants in the GPCRs it

296   ferries out of cilia (Jin et al., 2010; Klink et al., 2017; Ye et al., 2018; Seo et al., 2011; Domire et

297   al., 2011). We propose that the summation of weak molecular interactions between the BBSome

298   and UbK63 chains on one hand and the BBSome and GPCRs cytoplasmic loops on the other

299   hand increases the BBSome-cargo interaction to enable sorting of ubiquitinated GPCRs out of

300   cilia. In support of this bivalent recognition of ubiquitinated cargoes by the BBSome, the affinity

301   of the BBSome for cytoplasmic determinant of GPCRs are in the μM range (Klink et al., 2017)

302   and affinities of ubiquitin-binding proteins for ubiquitin typically reside in the sub mM range

303   (Husnjak and Dikic, 2012). The nature of the biochemical entity that directly recognizes

304   ubiquitin, and in particular UbK63 chains remains to be determined: while the BBSome was

305   pulled down on Ub-agarose resin from trypanosome lysates (Langousis et al., 2016), no known

306   Ub-binding domain is found in the BBSome polypeptides. Furthermore, the IFT-A subunit IFT-

307   139 associates with ubiquitinated α-tubulin in ciliary extracts from *Chlamydomonas*, suggesting a

308   possible recognition of ubiquitin by IFT139 (Wang et al., 2019). Again, the absence of known

309   Ub-binding domain in the sequence of IFT139 presents a challenge to this hypothesis.

310

311   **Requirements for K63-linked ubiquitination in ciliary exit and sorting to the**

312   **lysosome**

313   Wang et al. (2019) found that α-tubulin is modified by UbK63 chains and not UbK48 chain

314   upon ciliary disassembly. The ubiquitin ligases that have been associated with ciliary clearance of

315   Patched 1 and of PDGFRαα specifically assemble UbK63 chains (Kim et al., 2015; Yue et al.,

14

316   2014; Schmid et al., 2018). The suppression of GPR161, SSTR3 and SMO exit by cilia-AMSH

317   (**Figure 4**) demonstrates that UbK63 chains are recognized inside cilia to direct trafficking out of

318   cilia. The milder exit defect observed when acceptor lysines are mutated on ciliary GPCRs

319   (**Figure 2**) than when cilia-AMSH is expressed (**Figure 4**) suggests that K63Ub chains added

320   onto other ciliary proteins besides GPCRs may participate in ciliary exit. A role for

321   ubiquitination of the ciliary transport machinery in exit is in line with the functional importance

322   of ubiquitination of the endolysosomal machinery in GPCR trafficking (Dores and Trejo, 2019).

323   β arrestin ubiquitination promotes internalization of the β_2-adrenergic receptor (β_2AR) (Shenoy

324   et al., 2001, 2007; Shenoy and Lefkowitz, 2003), ubiquitination of the ESCRT components Hrs

325   and STAM participates in sorting of the chemokine receptor CXCR4 into the MVB (Malik and

326   Marchese, 2010; Marchese et al., 2003) and ubiquitination of the ESCRT-III recruitment factor

327   ALIX enhances MVB sorting of the protease activated receptor PAR-1 (Dores et al., 2015).

328   The requirement for UbK63 chains in signal-dependent exit from the cilium contrasts with the

329   more limited role of ubiquitin and UbK63 chains in signal-dependent endocytosis of signaling

330   receptors at the plasma membrane in mammals. Although ubiquitination is a major driver of

331   endocytosis in yeast (Stringer and Piper, 2011; Piper et al., 2014), foundational studies on

332   epidermal growth factor receptor (EGFR) trafficking found that signal-dependent receptor

333   ubiquitination is not essential for internalization because it is redundant with other

334   internalization mechanisms (Goh et al., 2010; Huang et al., 2013; Fortian et al., 2015). Studies of

335   an EGFR-AMSH fusion found that UbK63 chains attached onto EGFR become increasingly

336   necessary as EGFR progresses along the degradative route and a strict requirement for K63-

337   linked ubiquitin chains is observed at the terminal step of EGFR sorting into the lumen of

338   multivesicular body (MVB) (Huang et al., 2013). A strict requirement for receptor ubiquitination

339   in degradative sorting but not in internalization can be generalized to nearly all GPCRs

340   (Skieterska et al., 2017), namely β_2AR (Shenoy et al., 2001), CXCR4 (Marchese and Benovic,

341   2001), μ opioid receptor (Hislop et al., 2011), κ opioid receptor (Li et al., 2008), δ opioid receptor

342   (Henry et al., 2011), neurokinin-1 receptor (Cottrell et al., 2006), protease activated receptor 2

343   (PAR-2) (Jacob et al., 2005) and vasopressin receptor 2 (V2R) (Martin et al., 2003). Similarly, we

15

344   find that SSTR3 endocytosis proceeds normally in the absence of SSTR3 ubiquitination (**Figure**

345   **2C-D**). Studying the importance of ubiquitin K63 in mammalian cells via genetics remains

346   challenging because of the multiple genes encoding Ub but in yeast strains expressing UbK63R

347   as the sole source of Ub, the Gap1 permease is internalized normally and fails to get sorted into

348   the MVB (Lauwers et al., 2009).

349   The parallels between sorting at the late endosome and ciliary trafficking extend to β arrestin-

350   directed ubiquitination. While β arrestin functions inside cilia to direct the addition of ubiquitin

351   onto activated SSTR3 and GPR161 (**Figures 5 and 6**), β arrestin-mediated ubiquitination

352   selectively affects sorting at the level of endosomes rather that at the plasma membrane for

353   activated CXCR4 (Bhandari et al., 2007), β$_2$AR (Shenoy et al., 2008) and V2R (Martin et al.,

354   2003) and β arrestin-mediated ubiquitination of CXCR4 was shown to take place on endosomes

355   (Malik and Marchese, 2010). In this context, the recognition of K63-linked ubiquitin chain inside

356   cilia may befit the endosomal origin of primary cilia (Sorokin, 1962; Westlake et al., 2011;

357   Mitchell, 2017).

358   The parallels between endosomal and ciliary trafficking lead us to speculate that some

359   ubiquitinated proteins might be accidentally sorted to cilia instead of late endosomes. These

360   proteins would then need to be retrieved from cilia by the BBSome. Thus, the Ub signal detected

361   in photoreceptor outer segment and in *Chlamydomonas* flagella might result from the accidental

362   import of ubiquitinated proteins into cilia rather than *in situ* ubiquitination of unwanted proteins

363   inside cilia.

364

365   **Potential coupling between BBSome-mediated exit and degradative sorting**

366   An interesting consideration is the relationship between ciliary exit and endo-lysosomal sorting. It

367   has been proposed that endocytosis of signaling receptors is intimately coupled to their exit from

368   cilia (Pedersen et al., 2016). However, single molecule imaging of GPR161 exiting cilia suggests

369   that activated GPR161 diffuses into the plasma membrane after it exits from the ciliary

370   compartment (Ye et al., 2018). Prior findings that worm mutants for BBSome or the ESCRT

16

371   machinery both fail to remove ciliary proteins fused to Ub from cilia (Hu et al., 2007; Xu et al.,

372   2015) suggest the provocative possibility that ciliary exit may be tightly coupled to degradative

373   sorting. Nonetheless, the hypothesis that interfering with UbK63 chain formation on ciliary

374   GPCRs indirectly blocks ciliary exit because of a primary defect in endocytosis can be rejected

375   because ubiquitination is not a major determinant of SSTR3 endocytosis and because cilia-

376   AMSH potently and specifically blocks the signal-dependent exit of ciliary GPCRs.

377   In this context, the contrast between the dramatic increase in ubiquitinated SSTR3 levels in *Arl6*

378   *$^{-/-}$* cells compared to WT cells even in the absence of stimulation (**Figure 1C-D**) and the modest

379   increase in ciliary Ub levels in *Arl6$^{-/-}$* cells compared to WT cells in the absence of stimulation

380   (**Figure 1A-B**) suggests that a considerable amount of ubiquitinated SSTR3 accumulates outside

381   of cilia in *Arl6$^{-/-}$* cells. One interpretation consistent with a direct coupling between ciliary exit

382   and degradation is that a small fraction of ubiquitinated SSTR3 escapes cilia in *Arl6$^{-/-}$* cells but

383   fails to reach to correct degradative route. In this interpretation, the BBSome would deliver its

384   cargoes to the ESCRT machinery for routing into the lysosomal degradative pathway.

385

Ubiquitination and control of the ciliary proteome

387   A role for ubiquitination in selecting unwanted proteins for removal from cilia may unify the

388   functions of the BBSome in signal-dependent retrieval of GPCRs and the constitutive clearance

389   of proteins that accidentally enter cilia. In both of these cases, unwanted ciliary proteins need to

390   be recognized as 'non-self' by a ciliary surveillance machinery. For GPCRs, β arrestin orchestrate

391   the recognition of activated GPCRs as unwanted by directing their ubiquitination. A fascinating

392   question for future investigations is how the more than 100 proteins that accumulate in outer

393   segments of *Bbs* photoreceptors are recognized as 'non-self' and tagged with ubiquitin.

394

REFERENCES

395

396 Anvarian, Z., K. Mykytyn, S. Mukhopadhyay, L.B. Pedersen, and S.T. Christensen. 2019.
397   Cellular signalling by primary cilia in development, organ function and disease. *Nat. Rev.*
398   *Nephrol.* doi:10.1038/s41581-019-0116-9.

399 Baker, S.A., M. Haeri, P. Yoo, S.M. Gospe, N.P. Skiba, B.E. Knox, and V.Y. Arshavsky. 2008.
400   The outer segment serves as a default destination for the trafficking of membrane proteins
401   in photoreceptors. *J. Cell Biol.* 183:485–498. doi:10.1083/jcb.200806009.

402 Bhandari, D., J. Trejo, J.L. Benovic, and A. Marchese. 2007. Arrestin-2 interacts with the
403   ubiquitin-protein isopeptide ligase atrophin-interacting protein 4 and mediates
404   endosomal sorting of the chemokine receptor CXCR4. *J. Biol. Chem.* 282:36971–36979.
405   doi:10.1074/jbc.M705085200.

406 Chiang, A.P., J.S. Beck, H. Yen, M.K. Tayeh, T.E. Scheetz, R.E. Swiderski, D.Y. Nishimura,
407   T.A. Braun, K.-Y.A. Kim, J. Huang, K. Elbedour, R. Carmi, D.C. Slusarski, T.L.
408   Casavant, E.M. Stone, and V.C. Sheffield. 2006. Homozygosity mapping with SNP
409   arrays identifies TRIM32, an E3 ubiquitin ligase, as a Bardet-Biedl syndrome gene
410   (BBS11). *Proc. Natl. Acad. Sci. U. S. A.* 103:6287–6292. doi:10.1073/pnas.0600158103.

411 Corbit, K.C., P. Aanstad, V. Singla, A.R. Norman, D.Y.R. Stainier, and J.F. Reiter. 2005.
412   Vertebrate Smoothened functions at the primary cilium. *Nature.* 437:1018–1021.
413   doi:10.1038/nature04117.

414 Cottrell, G.S., B. Padilla, S. Pikios, D. Roosterman, M. Steinhoff, D. Gehringer, E.F. Grady, and
415   N.W. Bunnett. 2006. Ubiquitin-dependent Down-regulation of the Neurokinin-1
416   Receptor. *J. Biol. Chem.* 281:27773–27783. doi:10.1074/jbc.M603369200.

417 Craige, B., J.M. Brown, and G.B. Witman. 2013. Isolation of Chlamydomonas Flagella. *Curr.*
418   *Protoc. Cell Biol.* 59:3.41.1-3.41.9. doi:10.1002/0471143030.cb0341s59.

419 Datta, P., C. Allamargot, J.S. Hudson, E.K. Andersen, S. Bhattarai, A.V. Drack, V.C. Sheffield,
420   and S. Seo. 2015. Accumulation of non-outer segment proteins in the outer segment
421   underlies photoreceptor degeneration in Bardet-Biedl syndrome. *Proc Natl Acad Sci U A.*
422   112:E4400–9. doi:10.1073/pnas.1510111112.

423 Domire, J.S., J.A. Green, K.G. Lee, A.D. Johnson, C.C. Askwith, and K. Mykytyn. 2011.
424   Dopamine receptor 1 localizes to neuronal cilia in a dynamic process that requires the
425   Bardet-Biedl syndrome proteins. *Cell. Mol. Life Sci. CMLS.* 68:2951–2960.
426   doi:10.1007/s00018-010-0603-4.

427   Dores, M.R., H. Lin, N. J Grimsey, F. Mendez, and J. Trejo. 2015. The α-arrestin ARRDC3
428   mediates ALIX ubiquitination and G protein-coupled receptor lysosomal sorting. *Mol.*
429   *Biol. Cell.* 26:4660–4673. doi:10.1091/mbc.E15-05-0284.

430   Dores, M.R., and J. Trejo. 2019. Endo-lysosomal sorting of G-protein-coupled receptors by
431   ubiquitin: Diverse pathways for G-protein-coupled receptor destruction and beyond.
432   *Traffic Cph. Den.* 20:101–109. doi:10.1111/tra.12619.

433   Emmerich, C.H., and P. Cohen. 2015. Optimising methods for the preservation, capture and
434   identification of ubiquitin chains and ubiquitylated proteins by immunoblotting. *Biochem.*
435   *Biophys. Res. Commun.* 466:1–14. doi:10.1016/j.bbrc.2015.08.109.

436   Fortian, A., L.K. Dionne, S.H. Hong, W. Kim, S.P. Gygi, S.C. Watkins, and A. Sorkin. 2015.
437   Endocytosis of Ubiquitylation-Deficient EGFR Mutants via Clathrin-Coated Pits is
438   Mediated by Ubiquitylation. *Traffic Cph. Den.* 16:1137–1154. doi:10.1111/tra.12314.

439   Fujimuro, M., H. Sawada, and H. Yokosawa. 1994. Production and characterization of
440   monoclonal antibodies specific to multi-ubiquitin chains of polyubiquitinated proteins.
441   *FEBS Lett.* 349:173–180. doi:10.1016/0014-5793(94)00647-4.

442   Gigante, E.D., and T. Caspary. 2020. Signaling in the primary cilium through the lens of the
443   Hedgehog pathway. *Wiley Interdiscip. Rev. Dev. Biol.* e377. doi:10.1002/wdev.377.

444   Goh, L.K., F. Huang, W. Kim, S. Gygi, and A. Sorkin. 2010. Multiple mechanisms collectively
445   regulate clathrin-mediated endocytosis of the epidermal growth factor receptor. *J. Cell*
446   *Biol.* 189:871–883. doi:10.1083/jcb.201001008.

447   Gorman, D.S., and R.P. Levine. 1965. Cytochrome f and plastocyanin: their sequence in the
448   photosynthetic electron transport chain of Chlamydomonas reinhardi. *Proc. Natl. Acad. Sci.*
449   *U. S. A.* 54:1665–1669. doi:10.1073/pnas.54.6.1665.

450   Green, J.A., C.L. Schmid, E. Bley, P.C. Monsma, A. Brown, L.M. Bohn, and K. Mykytyn. 2015.
451   Recruitment of β-Arrestin into Neuronal Cilia Modulates Somatostatin Receptor
452   Subtype 3 Ciliary Localization. *Mol. Cell. Biol.* 36:223–235. doi:10.1128/MCB.00765-15.

453   Haglund, K., S. Sigismund, S. Polo, I. Szymkiewicz, P.P. Di Fiore, and I. Dikic. 2003. Multiple
454   monoubiquitination of RTKs is sufficient for their endocytosis and degradation. *Nat. Cell*
455   *Biol.* 5:461–466. doi:10.1038/ncb983.

456   Henry, A.G., J.N. Hislop, J. Grove, K. Thorn, M. Marsh, and M. von Zastrow. 2012.
457   Regulation of endocytic clathrin dynamics by cargo ubiquitination. *Dev. Cell.* 23:519–532.
458   doi:10.1016/j.devcel.2012.08.003.

459   Henry, A.G., I.J. White, M. Marsh, M. von Zastrow, and J.N. Hislop. 2011. The Role of
460   Ubiquitination in Lysosomal Trafficking of δ-Opioid Receptors. *Traffic*. 12:170–184.
461   doi:10.1111/j.1600-0854.2010.01145.x.

462   Hislop, J.N., A.G. Henry, and M. von Zastrow. 2011. Ubiquitination in the first cytoplasmic loop
463   of μ-opioid receptors reveals a hierarchical mechanism of lysosomal down-regulation. *J.
464   Biol. Chem.* 286:40193–40204. doi:10.1074/jbc.M111.288555.

465   Howarth, M., and A.Y. Ting. 2008. Imaging proteins in live mammalian cells with biotin ligase
466   and monovalent streptavidin. *Nat. Protoc.* 3:534–545. doi:10.1038/nprot.2008.20.

467   Hu, J., S.G. Wittekind, and M.M. Barr. 2007. STAM and Hrs down-regulate ciliary TRP
468   receptors. *Mol. Biol. Cell.* 18:3277–3289. doi:10.1091/mbc.E07-03-0239.

469   Huang, F., X. Zeng, W. Kim, M. Balasubramani, A. Fortian, S.P. Gygi, N.A. Yates, and A.
470   Sorkin. 2013. Lysine 63-linked polyubiquitination is required for EGF receptor
471   degradation. *Proc. Natl. Acad. Sci.* 110:15722–15727. doi:10.1073/pnas.1308014110.

472   Huang, K., D.R. Diener, and J.L. Rosenbaum. 2009. The ubiquitin conjugation system is
473   involved in the disassembly of cilia and flagella. *J. Cell Biol.* 186:601–613.
474   doi:10.1083/jcb.200903066.

475   Husnjak, K., and I. Dikic. 2012. Ubiquitin-binding proteins: decoders of ubiquitin-mediated
476   cellular functions. *Annu. Rev. Biochem.* 81:291–322. doi:10.1146/annurev-biochem-
477   051810-094654.

478   Jacob, C., G.S. Cottrell, D. Gehringer, F. Schmidlin, E.F. Grady, and N.W. Bunnett. 2005. c-
479   Cbl mediates ubiquitination, degradation, and down-regulation of human protease-
480   activated receptor 2. *J. Biol. Chem.* 280:16076–16087. doi:10.1074/jbc.M500109200.

481   Jiang, W., X. Yao, Z. Shan, W. Li, Y. Gao, and Q. Zhang. 2019. E3 ligase Herc4 regulates
482   Hedgehog signalling through promoting Smoothened degradation. *J. Mol. Cell Biol.*
483   11:791–803. doi:10.1093/jmcb/mjz024.

484   Jin, H., S.R. White, T. Shida, S. Schulz, M. Aguiar, S.P. Gygi, J.F. Bazan, and M.V. Nachury.
485   2010. The conserved Bardet-Biedl syndrome proteins assemble a coat that traffics
486   membrane proteins to cilia. *Cell*. 141:1208–1219. doi:10.1016/j.cell.2010.05.015.

487   Kim, J., E.Y. C Hsia, A. Brigui, A. Plessis, P.A. Beachy, and X. Zheng. 2015. The role of ciliary
488   trafficking in Hedgehog receptor signaling. *Sci. Signal.* 8:ra55–ra55.
489   doi:10.1126/scisignal.aaa5622.

490   Klink, B.U., E. Zent, P. Juneja, A. Kuhlee, S. Raunser, and A. Wittinghofer. 2017. A
491   recombinant BBSome core complex and how it interacts with ciliary cargo. *eLife*. 6.
492   doi:10.7554/eLife.27434.

493   Langousis, G., M.M. Shimogawa, E.A. Saada, A.A. Vashisht, R. Spreafico, A.R. Nager, W.D.
494   Barshop, M.V. Nachury, J.A. Wohlschlegel, and K.L. Hill. 2016. Loss of the BBSome
495   perturbs endocytic trafficking and disrupts virulence of Trypanosoma brucei. *Proc Natl*
496   *Acad Sci U A*. 113:632–637. doi:10.1073/pnas.1518079113.

497   Lauwers, E., C. Jacob, and B. André. 2009. K63-linked ubiquitin chains as a specific signal for
498   protein sorting into the multivesicular body pathway. *J. Cell Biol.* 185:493–502.
499   doi:10.1083/jcb.200810114.

500   Lechtreck, K.-F., E.C. Johnson, T. Sakai, D. Cochran, B.A. Ballif, J. Rush, G.J. Pazour, M.
501   Ikebe, and G.B. Witman. 2009. The Chlamydomonas reinhardtii BBSome is an IFT
502   cargo required for export of specific signaling proteins from flagella. *J. Cell Biol.*
503   187:1117–1132. doi:10.1083/jcb.200909183.

504   Li, J.-G., D.S. Haines, and L.-Y. Liu-Chen. 2008. Agonist-Promoted Lys63-Linked
505   Polyubiquitination of the Human κ-Opioid Receptor Is Involved in Receptor Down-
506   Regulation. *Mol. Pharmacol.* 73:1319–1330. doi:10.1124/mol.107.042846.

507   Liew, G.M., F. Ye, A.R. Nager, J.P. Murphy, J.S. Lee, M. Aguiar, D. Breslow, S.P. Gygi, and
508   M.V. Nachury. 2014. The intraflagellar transport protein IFT27 promotes BBSome exit
509   from cilia through the GTPase ARL6/BBS3. *Dev. Cell.* 31:265–278.
510   doi:10.1016/j.devcel.2014.09.004.

511   Loktev, A.V., and P.K. Jackson. 2013. Neuropeptide Y family receptors traffic via the Bardet-
512   Biedl syndrome pathway to signal in neuronal primary cilia. *Cell Rep.* 5:1316–1329.
513   doi:10.1016/j.celrep.2013.11.011.

514   Malik, R., and A. Marchese. 2010. Arrestin-2 interacts with the endosomal sorting complex
515   required for transport machinery to modulate endosomal sorting of CXCR4. *Mol. Biol.*
516   *Cell.* 21:2529–2541. doi:10.1091/mbc.e10-02-0169.

517   Marchese, A., and J.L. Benovic. 2001. Agonist-promoted ubiquitination of the G protein-coupled
518   receptor CXCR4 mediates lysosomal sorting. *J. Biol. Chem.* 276:45509–45512.
519   doi:10.1074/jbc.C100527200.

520   Marchese, A., C. Raiborg, F. Santini, J.H. Keen, H. Stenmark, and J.L. Benovic. 2003. The E3
521   ubiquitin ligase AIP4 mediates ubiquitination and sorting of the G protein-coupled
522   receptor CXCR4. *Dev. Cell.* 5:709–722. doi:10.1016/s1534-5807(03)00321-6.

523   Martin, N.P., R.J. Lefkowitz, and S.K. Shenoy. 2003. Regulation of V2 Vasopressin Receptor
524   Degradation by Agonist-promoted Ubiquitination. *J. Biol. Chem.* 278:45954–45959.
525   doi:10.1074/jbc.M308285200.

526   McCullough, J., M.J. Clague, and S. Urbé. 2004. AMSH is an endosome-associated ubiquitin
527   isopeptidase. *J. Cell Biol.* 166:487–492. doi:10.1083/jcb.200401141.

528   McCullough, J., P.E. Row, Ó. Lorenzo, M. Doherty, R. Beynon, M.J. Clague, and S. Urbé.
529   2006. Activation of the Endosome-Associated Ubiquitin Isopeptidase AMSH by STAM,
530   a Component of the Multivesicular Body-Sorting Machinery. *Curr. Biol.* 16:160–165.
531   doi:10.1016/j.cub.2005.11.073.

532   Michel, M.A., P.R. Elliott, K.N. Swatek, M. Simicek, J.N. Pruneda, J.L. Wagstaff, S.M.V.
533   Freund, and D. Komander. 2015. Assembly and specific recognition of k29- and k33-
534   linked polyubiquitin. *Mol. Cell.* 58:95–109. doi:10.1016/j.molcel.2015.01.042.

535   Milenkovic, L., L.E. Weiss, J. Yoon, T.L. Roth, Y.S. Su, S.J. Sahl, M.P. Scott, and W.E.
536   Moerner. 2015. Single-molecule imaging of Hedgehog pathway protein Smoothened in
537   primary cilia reveals binding events regulated by Patched1. *Proc Natl Acad Sci U A.*
538   112:8320–8325. doi:10.1073/pnas.1510094112.

539   Mitchell, D.R. 2017. Evolution of Cilia. *Cold Spring Harb. Perspect. Biol.* 9:a028290.
540   doi:10.1101/cshperspect.a028290.

541   Mukhopadhyay, S., X. Wen, N. Ratti, A. Loktev, L. Rangell, S.J. Scales, and P.K. Jackson.
542   2013. The ciliary G-protein-coupled receptor Gpr161 negatively regulates the Sonic
543   hedgehog pathway via cAMP signaling. *Cell.* 152:210–223.
544   doi:10.1016/j.cell.2012.12.026.

545   Mykytyn, K., and C. Askwith. 2017. G-Protein-Coupled Receptor Signaling in Cilia. *Cold Spring*
546   *Harb. Perspect. Biol.* a028183. doi:10.1101/cshperspect.a028183.

547   Mykytyn, K., R.F. Mullins, R.F. Mullins, M. Andrews, M. Andrews, A.P. Chiang, A.P. Chiang,
548   R.E. Swiderski, R.E. Swiderski, B. Yang, B. Yang, T. Braun, T. Braun, T. Casavant, T.
549   Casavant, E.M. Stone, E.M. Stone, and V.C. Sheffield. 2004. Bardet-Biedl syndrome
550   type 4 (BBS4)-null mice implicate Bbs4 in flagella formation but not global cilia assembly.
551   *Proc. Natl. Acad. Sci. U. S. A.* 101:8664–8669. doi:10.1073/pnas.0402354101.

552   Nachury, M.V. 2018. The molecular machines that traffic signaling receptors into and out of
553   cilia. *Curr. Opin. Cell Biol.* 51:124–131. doi:10.1016/j.ceb.2018.03.004.

554   Nachury, M.V., and D.U. Mick. 2019. Establishing and regulating the composition of cilia for
555   signal transduction. *Nat. Rev. Mol. Cell Biol.* 20:389–405. doi:10.1038/s41580-019-0116-4.

556   Nager, A.R., J.S. Goldstein, V. Herranz-Pérez, D. Portran, F. Ye, J.M. García-Verdugo, and
557   M.V. Nachury. 2017. An Actin Network Dispatches Ciliary GPCRs into Extracellular
558   Vesicles to Modulate Signaling. *Cell.* 168:252–263.e14. doi:10.1016/j.cell.2016.11.036.

559   Nakata, K., D. Shiba, D. Kobayashi, and T. Yokoyama. 2012. Targeting of Nphp3 to the
560   primary cilia is controlled by an N-terminal myristoylation site and coiled-coil domains.
561   *Cytoskelet. Hoboken NJ.* 69:221–234. doi:10.1002/cm.21014.

562   Newton, K., M.L. Matsumoto, I.E. Wertz, D.S. Kirkpatrick, J.R. Lill, J. Tan, D. Dugger, N.
563   Gordon, S.S. Sidhu, F.A. Fellouse, L. Komuves, D.M. French, R.E. Ferrando, C. Lam,
564   D. Compaan, C. Yu, I. Bosanac, S.G. Hymowitz, R.F. Kelley, and V.M. Dixit. 2008.
565   Ubiquitin chain editing revealed by polyubiquitin linkage-specific antibodies. *Cell.*
566   134:668–678. doi:10.1016/j.cell.2008.07.039.

567   Ocbina, P.J.R., and K.V. Anderson. 2008. Intraflagellar transport, cilia, and mammalian
568   Hedgehog signaling: analysis in mouse embryonic fibroblasts. *Dev. Dyn.* 237:2030–2038.
569   doi:10.1002/dvdy.21551.

570   Pal, K., S. Hwang, B. Somatilaka, H. Badgandi, P.K. Jackson, K. DeFea, and S.
571   Mukhopadhyay. 2016. Smoothened determines β-arrestin-mediated removal of the G
572   protein-coupled receptor Gpr161 from the primary cilium. *J. Cell Biol.* 212:861–875.
573   doi:10.1083/jcb.201506132.

574   Pedersen, L.B., J.B. Mogensen, and S.T. Christensen. 2016. Endocytic Control of Cellular
575   Signaling at the Primary Cilium. *Trends Biochem. Sci.* 41:784–797.
576   doi:10.1016/j.tibs.2016.06.002.

577   Piper, R.C., I. Dikic, and G.L. Lukacs. 2014. Ubiquitin-Dependent Sorting in Endocytosis. *Cold*
578   *Spring Harb. Perspect. Biol.* 6:a016808–a016808. doi:10.1101/cshperspect.a016808.

579   Postma, M., and J. Goedhart. 2019. PlotsOfData-A web app for visualizing data together with
580   their summaries. *PLoS Biol.* 17:e3000202. doi:10.1371/journal.pbio.3000202.

581   Rohatgi, R., L. Milenkovic, and M.P. Scott. 2007. Patched1 regulates hedgehog signaling at the
582   primary cilium. *Sci. N. Y. NY.* 317:372–376. doi:10.1126/science.1139740.

583   Sato, Y., A. Yoshikawa, A. Yamagata, H. Mimura, M. Yamashita, K. Ookata, O. Nureki, K.
584   Iwai, M. Komada, and S. Fukai. 2008. Structural basis for specific cleavage of Lys 63-
585   linked polyubiquitin chains. *Nature.* 455:358–362. doi:10.1038/nature07254.

586   Schmid, F.M., K.B. Schou, M.J. Vilhelm, M.S. Holm, L. Breslin, P. Farinelli, L.A. Larsen, J.S.
587   Andersen, L.B. Pedersen, and S.T. Christensen. 2018. IFT20 modulates ciliary PDGFRα
588   signaling by regulating the stability of Cbl E3 ubiquitin ligases. *J. Cell Biol.* 217:151–161.
589   doi:10.1083/jcb.201611050.

23

590   Seo, S., Q. Zhang, K. Bugge, D. Breslow, C.C. Searby, M.V. Nachury, and V.C. Sheffield.
591   2011. A novel protein LZTFL1 regulates ciliary trafficking of the BBSome and
592   Smoothened. *PLoS Genet.* 7:e1002358. doi:10.1371/journal.pgen.1002358.

593   Shaner, N.C., G.G. Lambert, A. Chammas, Y. Ni, P.J. Cranfill, M.A. Baird, B.R. Sell, J.R.
594   Allen, R.N. Day, M. Israelsson, M.W. Davidson, and J. Wang. 2013. A bright
595   monomeric green fluorescent protein derived from Branchiostoma lanceolatum. *Nat.*
596   *Methods*. 10:407–409. doi:10.1038/nmeth.2413.

597   Shankar, H., H. Shankar, A. Michal, A. Michal, R.C. Kern, R.C. Kern, D.S. Kang, D.S. Kang,
598   V.V. Gurevich, V.V. Gurevich, and J.L. Benovic. 2010. Non-visual arrestins are
599   constitutively associated with the centrosome and regulate centrosome function. *J. Biol.*
600   *Chem.* 285:8316–8329. doi:10.1074/jbc.M109.062521.

601   Shearer, R.F., and D.N. Saunders. 2016. Regulation of primary cilia formation by the ubiquitin-
602   proteasome system. *Biochem. Soc. Trans.* 44:1265–1271. doi:10.1042/BST20160174.

603   Shenoy, S.K., L.S. Barak, K. Xiao, S. Ahn, M. Berthouze, A.K. Shukla, L.M. Luttrell, and R.J.
604   Lefkowitz. 2007. Ubiquitination of beta-arrestin links seven-transmembrane receptor
605   endocytosis and ERK activation. *J. Biol. Chem.* 282:29549–29562.
606   doi:10.1074/jbc.M700852200.

607   Shenoy, S.K., and R.J. Lefkowitz. 2003. Trafficking Patterns of β-Arrestin and G Protein-
608   coupled Receptors Determined by the Kinetics of β-Arrestin Deubiquitination. *J. Biol.*
609   *Chem.* 278:14498–14506. doi:10.1074/jbc.M209626200.

610   Shenoy, S.K., P.H. McDonald, T.A. Kohout, and R.J. Lefkowitz. 2001. Regulation of receptor
611   fate by ubiquitination of activated beta 2-adrenergic receptor and beta-arrestin. *Science*.
612   294:1307–1313. doi:10.1126/science.1063866.

613   Shenoy, S.K., K. Xiao, V. Venkataramanan, P.M. Snyder, N.J. Freedman, and A.M. Weissman.
614   2008. Nedd4 mediates agonist-dependent ubiquitination, lysosomal targeting, and
615   degradation of the beta2-adrenergic receptor. *J. Biol. Chem.* 283:22166–22176.
616   doi:10.1074/jbc.M709668200.

617   Skieterska, K., P. Rondou, and K. Van Craenenbroeck. 2017. Regulation of G Protein-Coupled
618   Receptors by Ubiquitination. *Int. J. Mol. Sci.* 18. doi:10.3390/ijms18050923.

619   Sorokin, S. 1962. Centrioles and the formation of rudimentary cilia by fibroblasts and smooth
620   muscle cells. *J. Cell Biol.* 15:363–377. doi:10.1083/jcb.15.2.363.

621   Stringer, D.K., and R.C. Piper. 2011. A single ubiquitin is sufficient for cargo protein entry into
622   MVBs in the absence of ESCRT ubiquitination. *J. Cell Biol.* 192:229–242.
623   doi:10.1083/jcb.201008121.

624   Swatek, K.N., and D. Komander. 2016. Ubiquitin modifications. *Cell Res.* 26:399–422.
625   doi:10.1038/cr.2016.39.

626   Wang, Q., Z. Peng, H. Long, X. Deng, and K. Huang. 2019. Polyubiquitylation of α-tubulin at
627   K304 is required for flagellar disassembly in Chlamydomonas. *J. Cell Sci.* 132.
628   doi:10.1242/jcs.229047.

629   Westlake, C.J., L.M. Baye, M.V. Nachury, K.J. Wright, K.E. Ervin, L. Phu, C. Chalouni, J.S.
630   Beck, D.S. Kirkpatrick, D.C. Slusarski, V.C. Sheffield, R.H. Scheller, and P.K. Jackson.
631   2011. Primary cilia membrane assembly is initiated by Rab11 and transport protein
632   particle II (TRAPPII) complex-dependent trafficking of Rabin8 to the centrosome. *Proc*
633   *Natl Acad Sci U A.* 108:2759–2764. doi:10.1073/pnas.1018823108.

634   Wingfield, J.L., K.-F. Lechtreck, and E. Lorentzen. 2018. Trafficking of ciliary membrane
635   proteins by the intraflagellar transport/BBSome machinery. *Essays Biochem.* 62:753–763.
636   doi:10.1042/EBC20180030.

637   Wright, K.J., L.M. Baye, A. Olivier-Mason, S. Mukhopadhyay, L. Sang, M. Kwong, W. Wang,
638   P.R. Pretorius, V.C. Sheffield, P. Sengupta, D.C. Slusarski, and P.K. Jackson. 2011. An
639   ARL3-UNC119-RP2 GTPase cycle targets myristoylated NPHP3 to the primary cilium.
640   *Genes Dev.* 25:2347–2360. doi:10.1101/gad.173443.111.

641   Xia, R., H. Jia, J. Fan, Y. Liu, and J. Jia. 2012. USP8 promotes smoothened signaling by
642   preventing its ubiquitination and changing its subcellular localization. *PLoS Biol.*
643   10:e1001238. doi:10.1371/journal.pbio.1001238.

644   Xu, Q., Y. Zhang, Q. Wei, Y. Huang, Y. Li, K. Ling, and J. Hu. 2015. BBS4 and BBS5 show
645   functional redundancy in the BBSome to regulate the degradative sorting of ciliary
646   sensory receptors. *Sci. Rep.* 5:11855. doi:10.1038/srep11855.

647   Yau, R., and M. Rape. 2016. The increasing complexity of the ubiquitin code. *Nat. Cell Biol.*
648   18:579–586. doi:10.1038/ncb3358.

649   Ye, F., A.R. Nager, and M.V. Nachury. 2018. BBSome trains remove activated GPCRs from
650   cilia by enabling passage through the transition zone. *J. Cell Biol.* 217:1847–1868.
651   doi:10.1083/jcb.201709041.

652   Yue, S., L.-Y. Tang, Y. Tang, Y. Tang, Q.-H. Shen, J. Ding, Y. Chen, Z. Zhang, T.-T. Yu, Y.E.
653   Zhang, and S.Y. Cheng. 2014. Requirement of Smurf-mediated endocytosis of Patched1
654   in sonic hedgehog signal reception. *eLife.* 3:128. doi:10.7554/eLife.02555.

655   Zhang, Q., D. Nishimura, S. Seo, T. Vogel, D.A. Morgan, C. Searby, K. Bugge, E.M. Stone, K.
656   Rahmouni, and V.C. Sheffield. 2011. Bardet-Biedl syndrome 3 (Bbs3) knockout mouse

657   model reveals common BBS-associated phenotypes and Bbs3 unique phenotypes. *Proc*

658   *Natl Acad Sci U A*. 108:20678–20683. doi:10.1073/pnas.1113220108.

659

660

661   **ACKNOWLEDGMENTS**

675

27

Figure 1

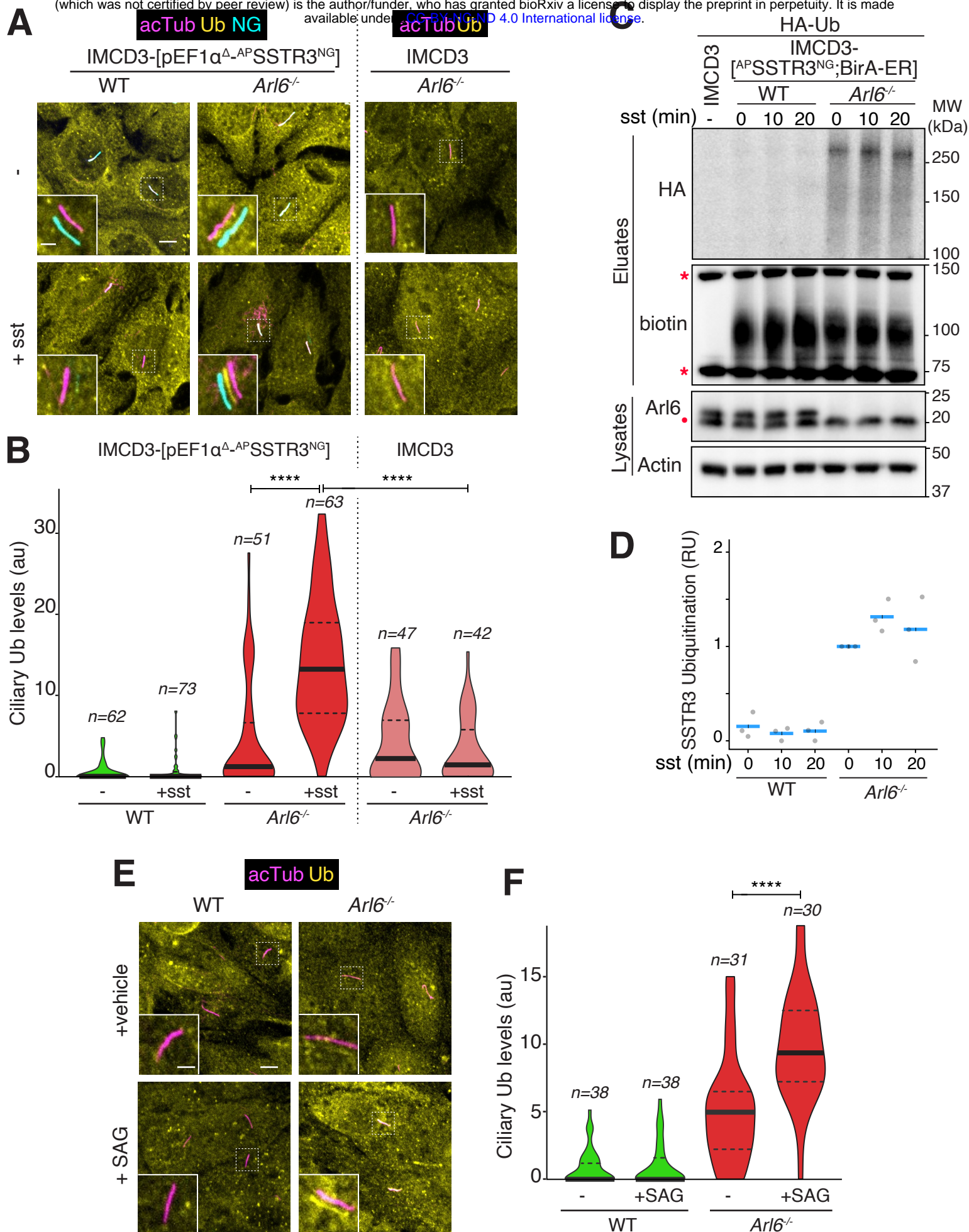**Figure 1. Ubiquitinated signaling receptors accumulate inside cilia of *Arl6⁻/⁻* cells**

A. SSTR3 fused to the fluorescent protein mNeonGreen (NG) at its intracellular C-terminus and a biotinylation Acceptor Peptide (AP) tag at its extracellular N-terminus was expressed under the control of an attenuated EF1α promoter (pEF1α^A) in wild type (WT) and *Arl6⁻/⁻* IMCD3 cells. Cells were treated with or without somatostatin-14 (sst) for 2 h, then fixed and stained for acetylated tubulin (acTub, magenta) and ubiquitin (Ub, yellow). ^{AP}SSTR3^{NG} (cyan) was imaged through the intrinsic fluorescence of NG. Channels are shifted in the insets to facilitate visualization of overlapping ciliary signals. Scale bar: 5µm (main panel), 2µm (inset). In WT cells, the ciliary SSTR3 signal decreases over the experimental time course. In *Arl6⁻/⁻* cells, SSTR3 fails to exit cilia and an increase in the ciliary Ub level is detected. As a control, *Arl6⁻/⁻* cells that did not express SSTR3-NG were tested; no increase in ciliary Ub levels was observed upon addition of sst. **B.** The fluorescence intensity of the Ub channel in the cilium was measured in each condition and the data are represented as violin plots. The thick bar indicates the median and the dotted lines the first and third quartiles. An 11-fold increase in ciliary Ub signal is observed upon addition of sst to SSTR3-expressing cells. Asterisks indicate ANOVA significance value. ****, p= <0.0001. **C.** WT or *Arl6⁻/⁻* IMCD3 cells stably expressing ^{AP}SSTR3^{NG} and the biotin ligase BirA targeted to the ER lumen (BirA-ER) were transiently transfected with HA-tagged ubiquitin (HA-Ub). 10 µM biotin was added to cells 24 h post transfection for maximal biotinylation of ^{AP}SSTR3^{NG} and, after another 18 h, cells were treated with sst (10µM) for indicated times. Cells were lysed under denaturing conditions and biotinylated SSTR3 was captured on streptavidin resin. Eluates were probed for HA via immunoblotting and for biotin via streptavidin-HRP. Two major biotinylated proteins endogenous to cells are marked by asterisks. Whole cell lysates were probed for Arl6 and, as a loading control, actin. A non-specific band cross-reacting with the anti-Arl6 antibody is marked with a dot. **D.** Quantitation of SSTR3 ubiquitination. The signals of HA-Ub conjugated to SSTR3 in the streptavidin eluates were measured. The experiment shown in **C** was repeated three times and for each experiment, Ub-SSTR3 signals were normalized to the value in *Arl6⁻/⁻* cells at t = 0 of sst stimulation and plotted as grey circles. The horizontal blue lines represent mean values. **E.** IMCD3 cells of the indicated genotypes were treated with the

28

704   Smoothened agonist SAG or the vehicle DMSO for 2h. Cells were then fixed and stained for

705   acTub and Ub. Channels are shifted in the insets to facilitate visualization of overlapping ciliary

706   signals. Scale bar 5µm (main panel), 2µm (inset). Activation of Hh signaling promotes a

707   detectable increase in ciliary Ub levels only in $Arl6^{-/-}$ cells. **F.** Violin plots of the fluorescence

708   intensity of the Ub channel in the cilium in each condition are shown. Asterisks indicate

709   ANOVA significance value. ****, p= <0.0001.

710

711
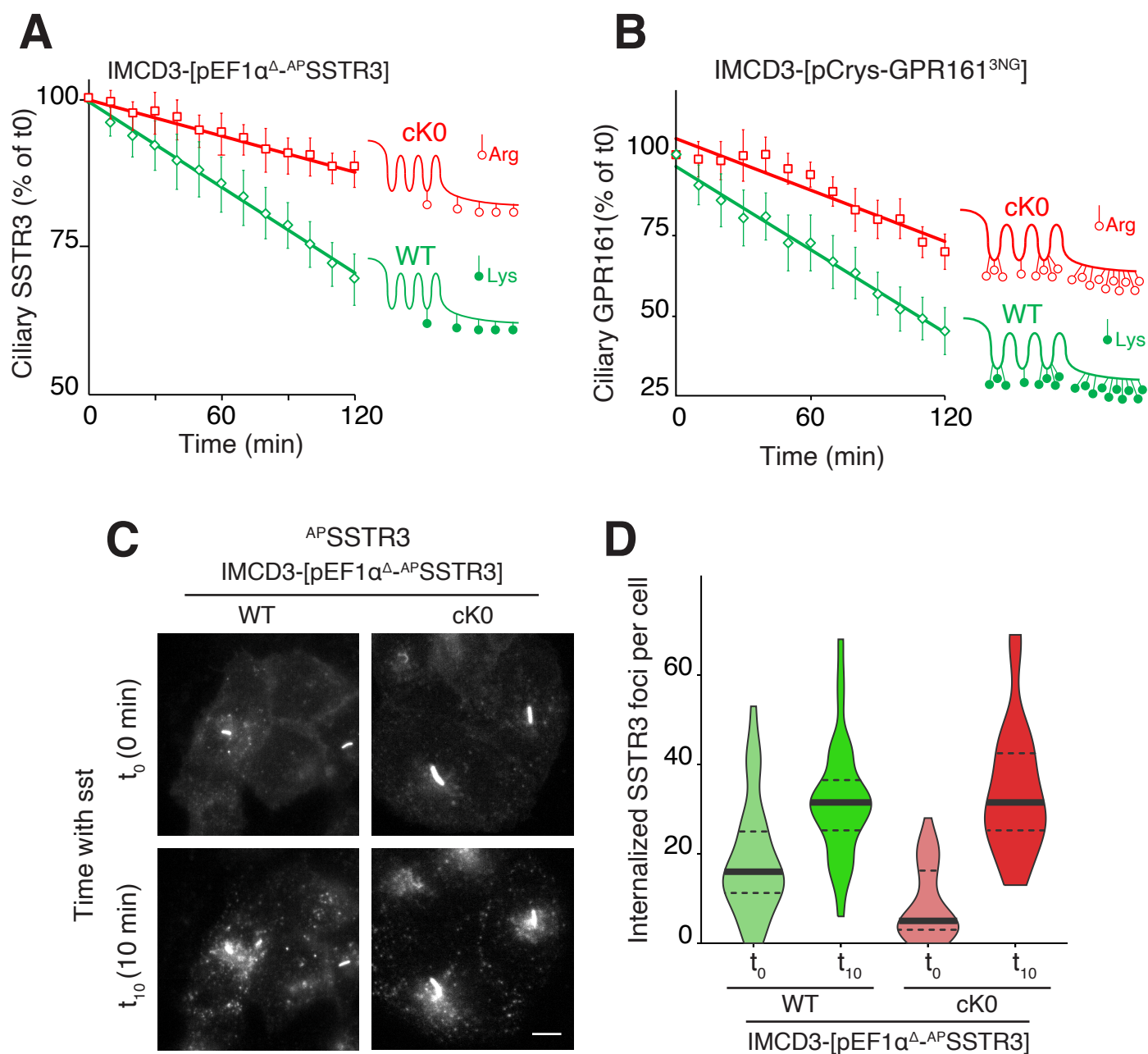
Figure 2

712 **Figure 2. Ubiquitination of ciliary GPCRs is required for signal-dependent exit but**

713 **not for endocytosis.**

714 **A.** IMCD3-[pEF1α$^{\Delta}$-^{AP}SSTR3] cells stably expressed the ER-localized biotin ligase BirA to

715 enables the biotinlylation of ^{AP}SSTR3. SSTR3 was either the wild-type allele (WT) or a variant

716 where all five cytoplasm-facing lysine residues (listed in Methods) were mutated to arginine (cK0).

717 Ciliary ^{AP}SSTR3 was pulse-labeled by addition of Alexa647-conjugated mSA (mSA647) to the

718 medium for 5-10 min before addition of sst. Far red fluorescence was tracked in individual cilia at

719 10 min capture intervals. For each individual cilia, fluorescence intensities were normalized to

720 the value at t = 0. A comparison of the ciliary levels of SSTR3 at t=0 is shown in **Fig. S2A**. Data

721 were plotted and fitted to a line. Error bars: 95% CI. $\mathcal{N}$ =18-22 cilia. **B.** GPR161 fused to three

722 tandem repeats of NG at its C-terminus was expressed under the control of the ultra-weak δ-

723 crystallin promoter (pCrys) in IMCD3 cells. GPR161 was either the wild-type allele (WT) or a

724 variant where all eighteen cytoplasm-facing lysine residues (listed in Methods) where mutated to

725 arginine (cK0). IMCD3-[pCrys-GPR161^{3NG}] cells were treated with SAG for 2h. During the

726 course of the experiment, NG fluorescence was tracked in individual cilia at 10 min capture

727 intervals. Fluorescence data were acquired and analyzed as in panel **(A)**. A comparison of the

728 ciliary levels of GPR161 at t=0 is shown in **Fig. S2B**. Error bars: 95% CI. $\mathcal{N}$ =10-19 cilia. **C.**

729 IMCD3-[^{AP}SSTR3; BirA-ER] cells expressing either WT or cK0 SSTR3 were pulse-labeled by

730 addition of Alexa647-conjugated mSA (mSA647) to the medium for 5 min before addition of sst

731 and were imaged by far red fluorescence immediately after addition of sst (t_0) and 10 min later

732 (t_{10}). The contrast level was adjusted to reveal plasma membrane-localized and internalized

733 ^{AP}SSTR3, causing the cilia-localized ^{AP}SSTR3 signal to reach saturation. Scale bar 5μm. **D.**

734 Internalized ^{AP}SSTR3 foci were counted immediately after addition of sst (t_0) and 10 min later
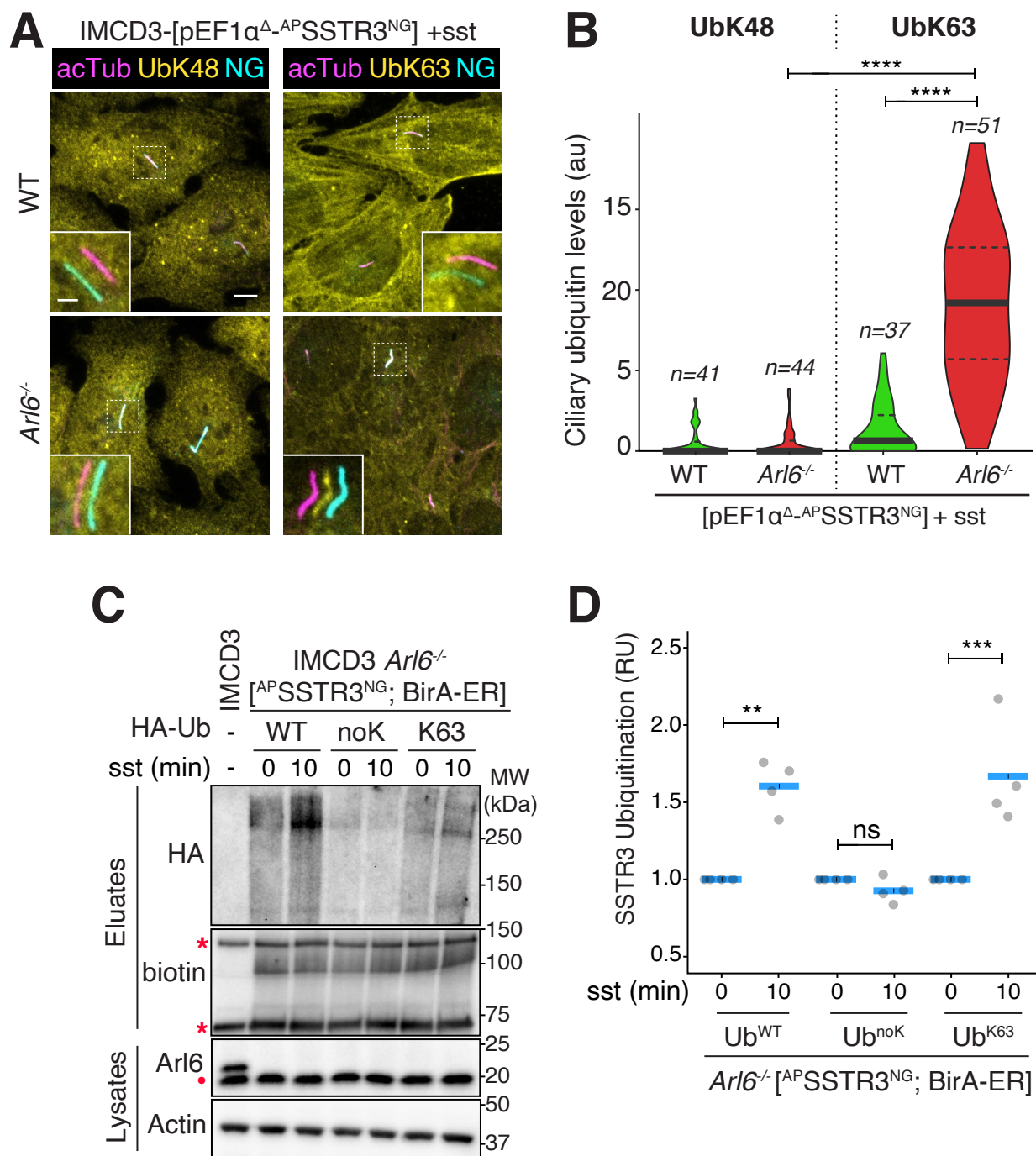
735 (t_{10}), n = 34 cells.

Figure 3

736 **Figure 3. Signal-dependent accumulation of K63-linked ubiquitin chains inside**

737 **cilia of *Bbs* mutant cells.**

738 **A.** IMCD3 cells of the indicated genotypes expressing ^{AP}SSTR3^{NG} were treated with

739 somatostatin-14 for 2 h. Cells were fixed and stained for AcTub (magenta) and with antibodies

740 specific for the lysine 63 (UbK63) or lysine 48 (UbK48) Ub chain linkages (yellow). SSTR3^{NG}

741 (cyan) was imaged through the intrinsic fluorescence of NG. Channels are shifted in the insets to

742 facilitate visualization of overlapping ciliary signals. Scale bar 5µm (main panel), 2µm (inset). **B.**

743 The fluorescence intensity of the UbK48 and UbK63 channels in the cilium are represented as

744 violin plots. A 14-fold increase in ciliary Ub abundance is detected with the K63Ub linkage-

745 specific antibody. Asterisks indicate ANOVA significance value. ****, p= <0.0001. No ciliary

746 signal is detected with the K48Ub linkage-specific antibody. **C.** *Arl6$^{-/-}$* IMCD3-[^{AP}SSTR3; BirA-

747 ER] cells were transfected with the HA-tagged ubiquitin variants WT, noK0 (all seven acceptor

748 lysine residues mutated to arginine) or K63 (where all lysine residues are mutated to arginine

749 except for K63). Biotin was included in the culture medium and cells were treated with sst for 0

750 or 10 min. Cells were lysed under denaturing conditions and biotinylated SSTR3 was captured

751 on streptavidin resin. Eluates were probed for HA via immunoblotting and for biotin via

752 streptavidin-HRP. Two major biotinylated proteins endogenous to cells are marked by asterisks.

753 Whole cell lysates were probed for Arl6 and, as a loading control, actin. A non-specific band

754 cross-reacting with the anti-Arl6 antibody is marked with a dot. WT IMCD3 cells were processed

755 in parallel as a control. **D.** Quantitation of SSTR3 ubiquitination. The signals of HA-Ub

756 conjugated to SSTR3 in the streptavidin eluates were measured. The experiment shown in **C**

757 was repeated four times and for each Ub variant, Ub-SSTR3 signals were normalized to the

758 value at t = 0 of sst stimulation and plotted as grey circles. The horizontal blue lines represent

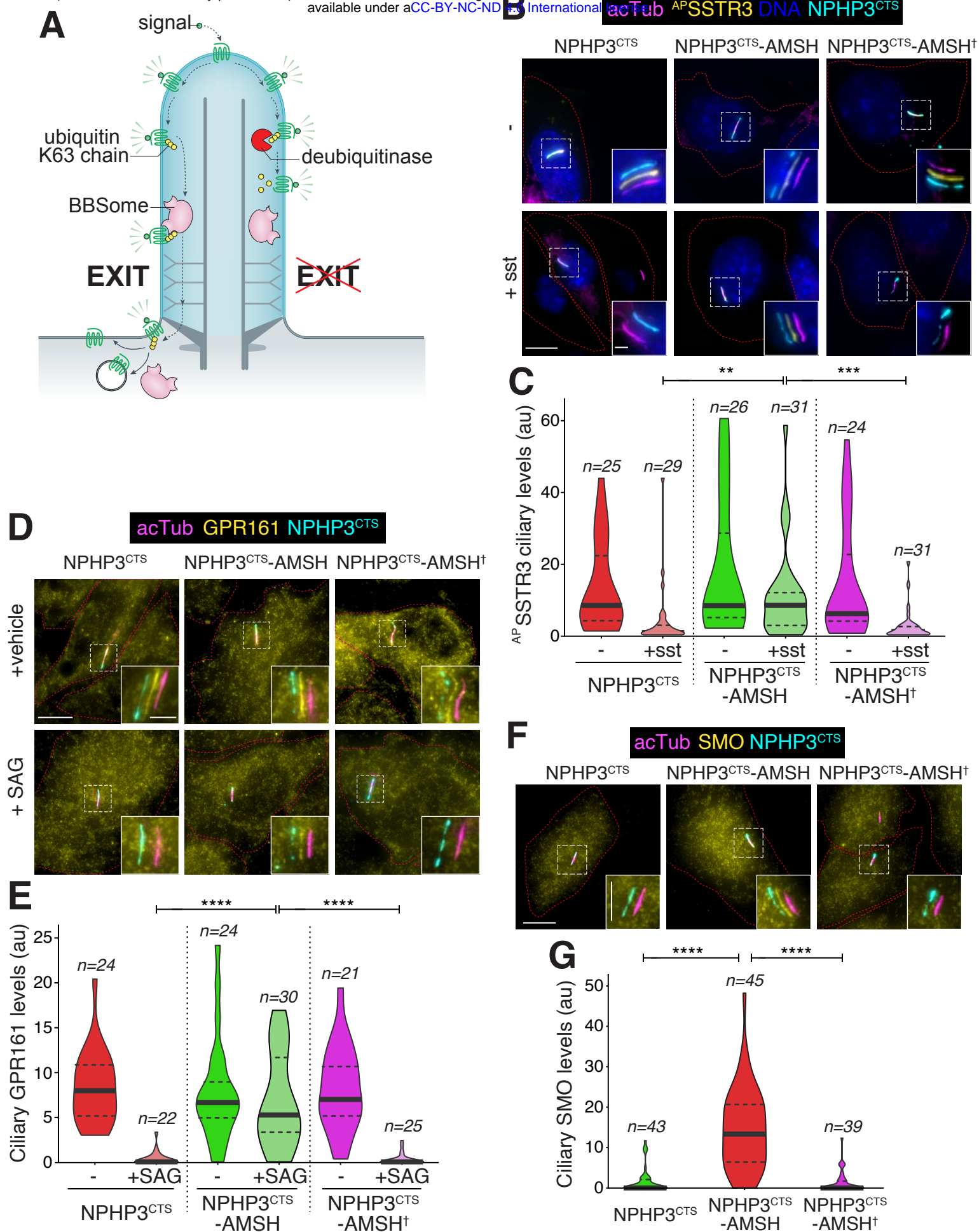759 mean values. Asterisks indicate ANOVA significance value. *** p =< 0.001; ** p=<0.01.

760

Figure 4

761 **Figure 4. Ciliary K63-linked ubiquitin chains are required for GPCR exit from**
762 **cilia.**

763 **A.** Diagram of the working model and the experimental strategy. **B.** IMCD3-[pEF1α$^\Delta$-
764 ^{AP}SSTR3; pEF1α-BirA•ER] were transfected with plasmids expressing the ciliary targeting signal
765 (CTS) of NPHP3 fused to GFP only (left panels), to GFP and the catalytic domain of the K63-
766 specific deubiquitinase AMSH (middle panels), or to GFP and the catalytically inactive E280A
767 variant of AMSH catalytic domain (AMSH†, right panels). Ciliary ^{AP}SSTR3 was pulse-labeled
768 with mSA647 for 5-10 min and cells were then treated with or without sst for 2h, before fixation
769 and staining for acetylated tubulin (acTub, magenta) and DNA (blue). The NPHP3^{CTS} fusions
770 were visualized through the intrinsic fluorescence of GFP (cyan) and ^{AP}SSTR3 was visualized via
771 mSA647 (yellow). Channels are shifted in the insets to facilitate visualization of overlapping
772 ciliary signals. Scale bar 5μm (main panel), 2μm (inset). **C.** The fluorescence intensities of ciliary
773 $^{mSA647-AP}$SSTR3 are represented as violin plots. Asterisks indicate Kruskal-Wallis test significance
774 values. *******, p= <0.001; ******, p= <0.01. Addition of sst triggers the exit of SSTR3 from cilia in cells
775 transfected with the controls NPHP3^{CTS} and NPHP3^{CTS}-AMSH† but NPHP3^{CTS}-AMSH blocks
776 ciliary exit of SSTR3. **D.** RPE1-hTERT (RPE) cells transfected with the indicated constructs
777 were treated with SAG or vehicle (DMSO) for 2h, then fixed and stained for acetylated tubulin
778 (magenta) and GPR161 (yellow). The NPHP3^{CTS} fusions were visualized through the intrinsic
779 fluorescence of GFP (cyan). Channels are shifted in the insets to facilitate visualization of
780 overlapping ciliary signals. Scale bar 5μm (main panel), 2μm (inset). **E.** The fluorescence
781 intensities of ciliary GPR161 are represented as violin plots. Asterisks indicate ANOVA
782 significance value. ********, p= <0.0001. NPHP3^{CTS}-AMSH specifically blocks the SAG-dependent
783 exit of GPR161 from cilia. **F.** IMCD3 cells transfected with the indicated constructs were fixed
784 and stained for acetylated tubulin (magenta) and SMO (yellow). The NPHP3^{CTS} fusions were
785 visualized through the intrinsic fluorescence of GFP (cyan). Channels are shifted in the insets to
786 facilitate visualization of overlapping ciliary signals. **G.** The fluorescence intensities of ciliary
787 SMO are represented as violin plots. Asterisks indicate ANOVA significance value. ********, p=

32

788 <0.0001. NPHP3$^{\mathrm{CTS}}$-AMSH specifically blocks the constitutive exit of SMO from cilia and

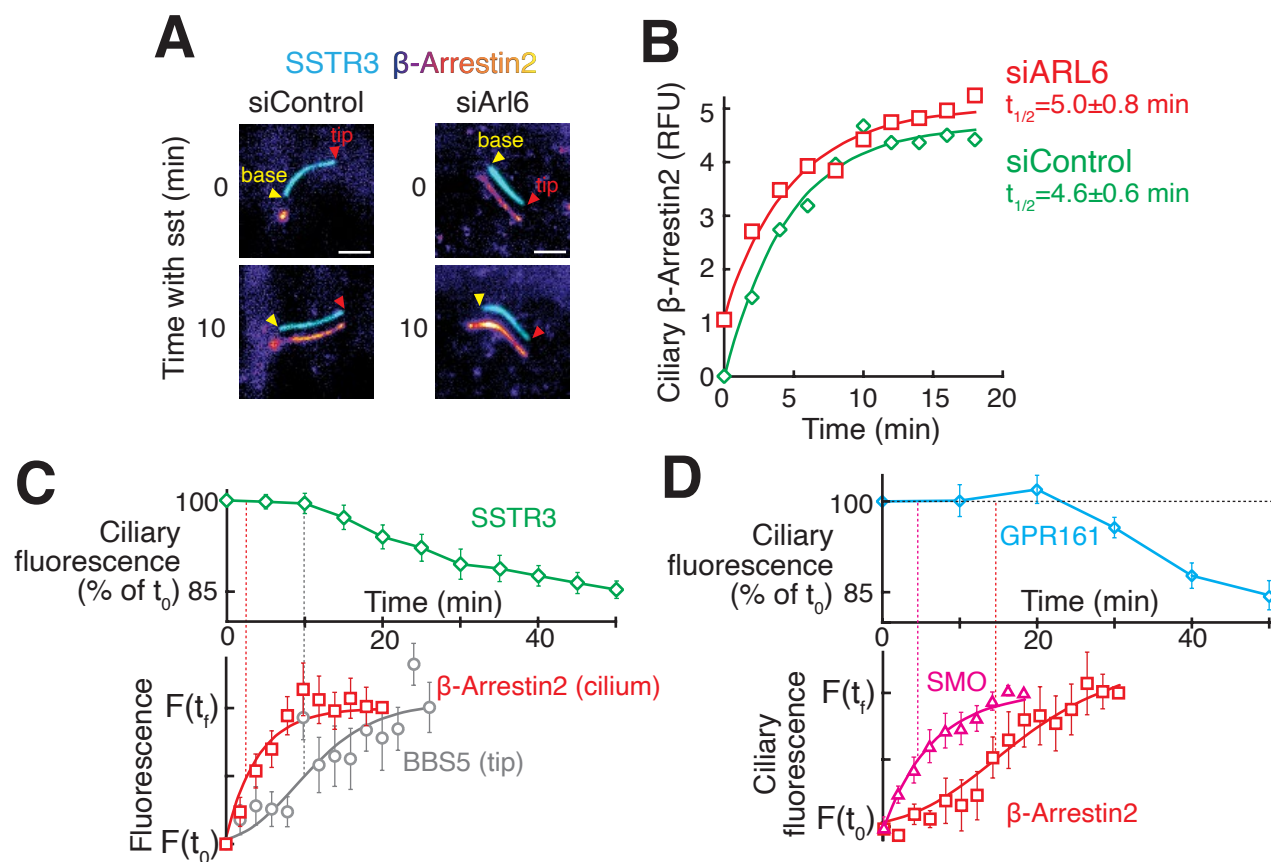789 promotes accumulation of SMO in cilia in the absence of pathway activation.

Figure 5

790   **Figure 5. β-arrestin 2 is recruited to cilia upon activation of SSTR3 or GPR161.**

791   **A.** β-Arrestin2 is rapidly recruited to cilia upon activation of SSTR3. siRNA-treated IMCD3-

792   [^{AP}SSTR3, β-Arrestin2^{GFP}] cells were pulse-labeled with mSA647 before addition of sst.

793   Channels are shifted to facilitate visualization of overlapping ciliary signals. As shown previously

794   (Shankar et al., 2010), β-Arrestin2 is at the basal body in unstimulated cells. Scale bar: 2 μm. **B.**

795   Kinetics of β-Arrestin2^{GFP} recruitment to cilia upon sst stimulation in control- and ARL6-

796   depleted IMCD3-[^{AP}SSTR3, β-Arrestin2^{GFP}] cells. Data were fit to a simple exponential. (n=10

797   cilia). **C-D.** Kinetics of early trafficking events for retrieval of SSTR3 **(C)** and GPR161 **(D)**. The

798   top panels show removal of stably expressed ^{AP}SSTR3^{NG} or ^{AP}GPR161^{NG3} following addition of

799   sst **(C)** or SAG **(D)**. The bottom panels show the kinetics of β-Arrestin2^{GFP} entry **(C-D)**,

800   ^{AP}Smoothened^{NG} entry **(D)**, and ^{NG3}BBS5 tip accumulation **(C)** measured in IMCD3 cells stably

801   expressing the indicated proteins. Fluorescence values are normalized to the initial (t_0) and final
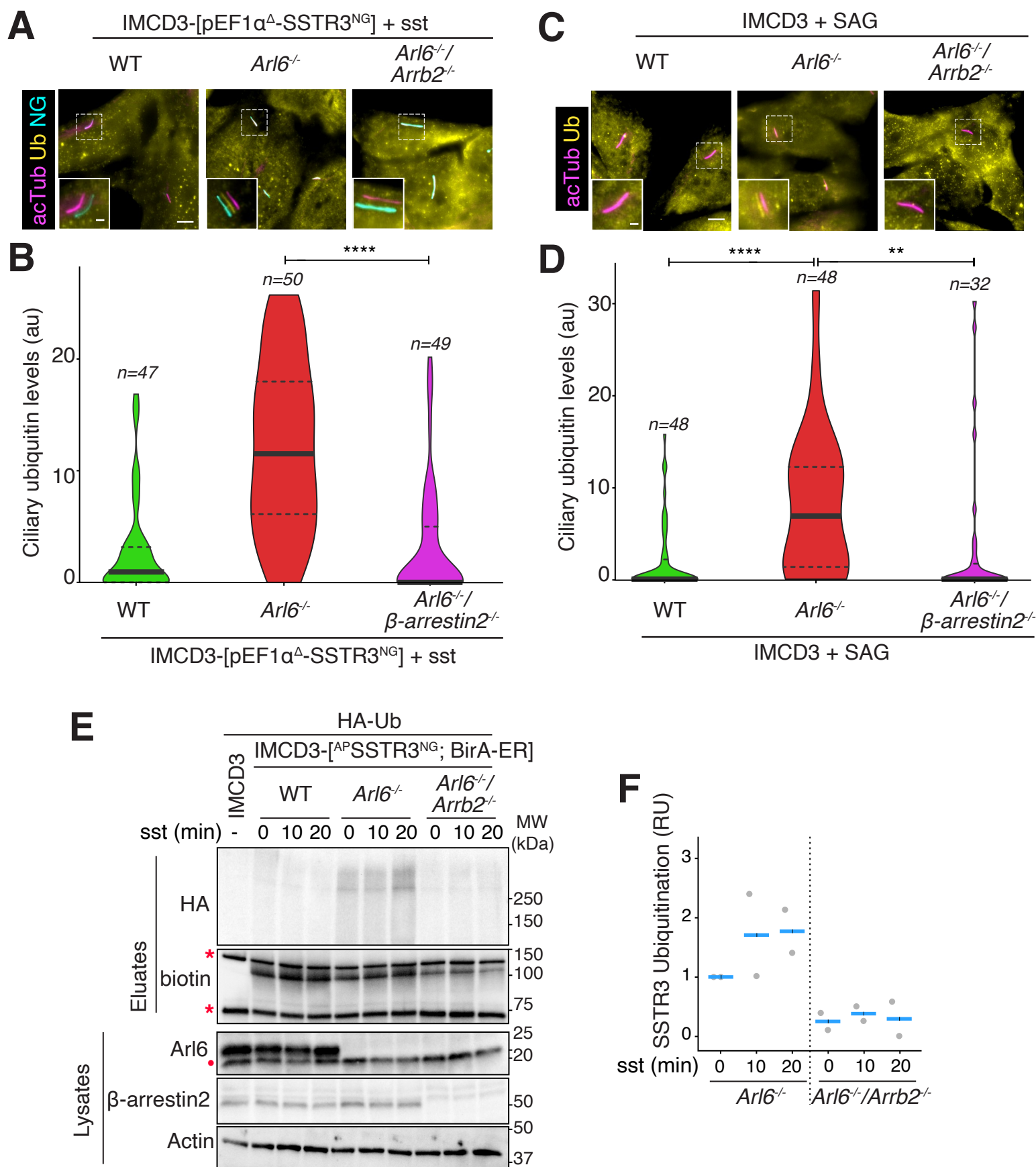
802   (t_f) values. Error bars: SEM. (n=6-11 cilia).

803

34

Figure 6

Figure 6. β-arrestin 2 directs the signal-dependent ubiquitination of ciliary GPCRs.

A. IMCD3-[pEF1α$^\Delta$-^{AP}SSTR3^{NG}] cells of the indicated genotypes were treated with sst for 2h before fixation and staining for acetylated tubulin (acTub, magenta) and ubiquitin (Ub, yellow). SSTR3^{NG} was visualized through the intrinsic fluorescence of NG (cyan). Channels are shifted in the insets to facilitate visualization of overlapping ciliary signals. SSTR3 exit is blocked in *Arl6$^{-/-}$* cells regardless of the *ß-Arrestin2* genotype but the ciliary Ub signal is only evident when β-Arrestin2 function is intact. Scale bar: 5µm (main panel), 1µm (inset). **B.** Violin plots representing the ciliary levels of Ub under the indicated conditions. Asterisks indicate ANOVA significance value. ****, p= <0.0001. **C.** IMCD3 WT, knockout for *Arl6* only and double knockout for *Arl6* and the β-Arrestin2 gene *Arrb2* were treated with SAG for 2h before fixation and staining for acetylated tubulin (acTub, magenta) and ubiquitin (Ub, yellow). Channels are shifted in the insets to facilitate visualization of overlapping ciliary signals. Scale bar: 5µm (main panel), 1µm (inset). **D.** Violin plots representing the ciliary Ub levels. Asterisks indicate ANOVA significance value. ****, p= <0.0001; **, p= <0.01. The appearance of a Ub signal in cilia in *Arl6$^{-/-}$* cells depends on β-Arrestin2. **E.** IMCD3-[^{AP}SSTR3; BirA-ER] cells of the indicated genotypes stably expressing ^{AP}SSTR3^{NG} and BirA-ER were transfected with HA-Ub, biotin was added to the medium and cells were treated with sst for indicated times. Biotinylated SSTR3 was captured from cell lysates under denaturing conditions on streptavidin resin. Eluates were probed for HA via immunoblotting and for biotin via streptavidin-HRP. Two major biotinylated proteins endogenous to cells are marked by asterisks. Whole cell lysates were probed for Arl6, β-Arrestin2 to verify genotypes and, as a loading control, actin. A non-specific band cross-reacting with the anti-Arl6 antibody is marked with a dot. WT IMCD3 cells were processed in parallel as a control. **F.** Quantitation of SSTR3 ubiquitination. The signals of HA-Ub conjugated to SSTR3 in the streptavidin eluates were measured. The experiment shown in **E** was repeated twice and for each experiment, Ub-SSTR3 signals were normalized to the value in *Arl6$^{-/-}$* cells at t = 0 of sst stimulation and plotted as grey circles. The horizontal blue lines represent mean values.
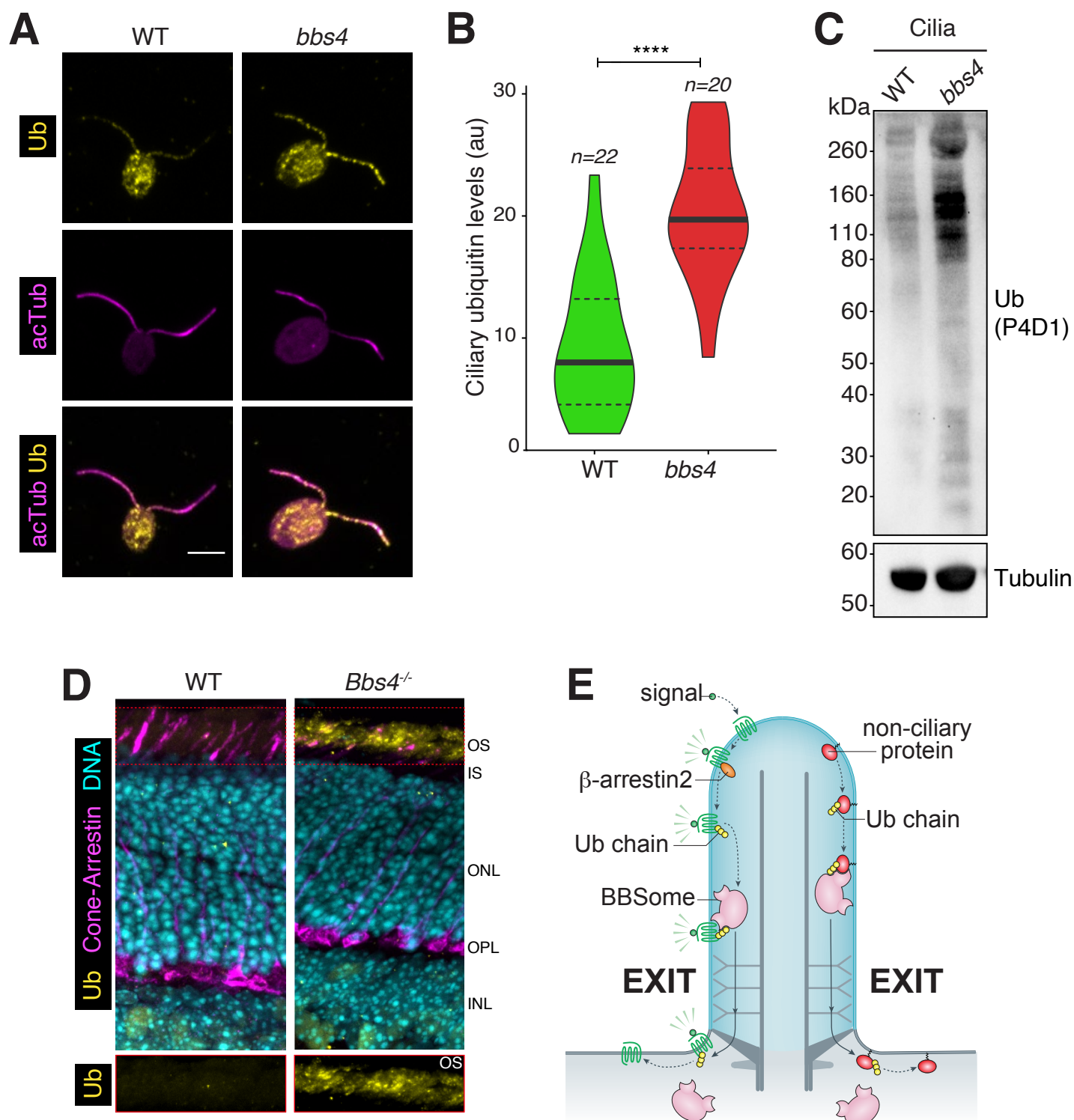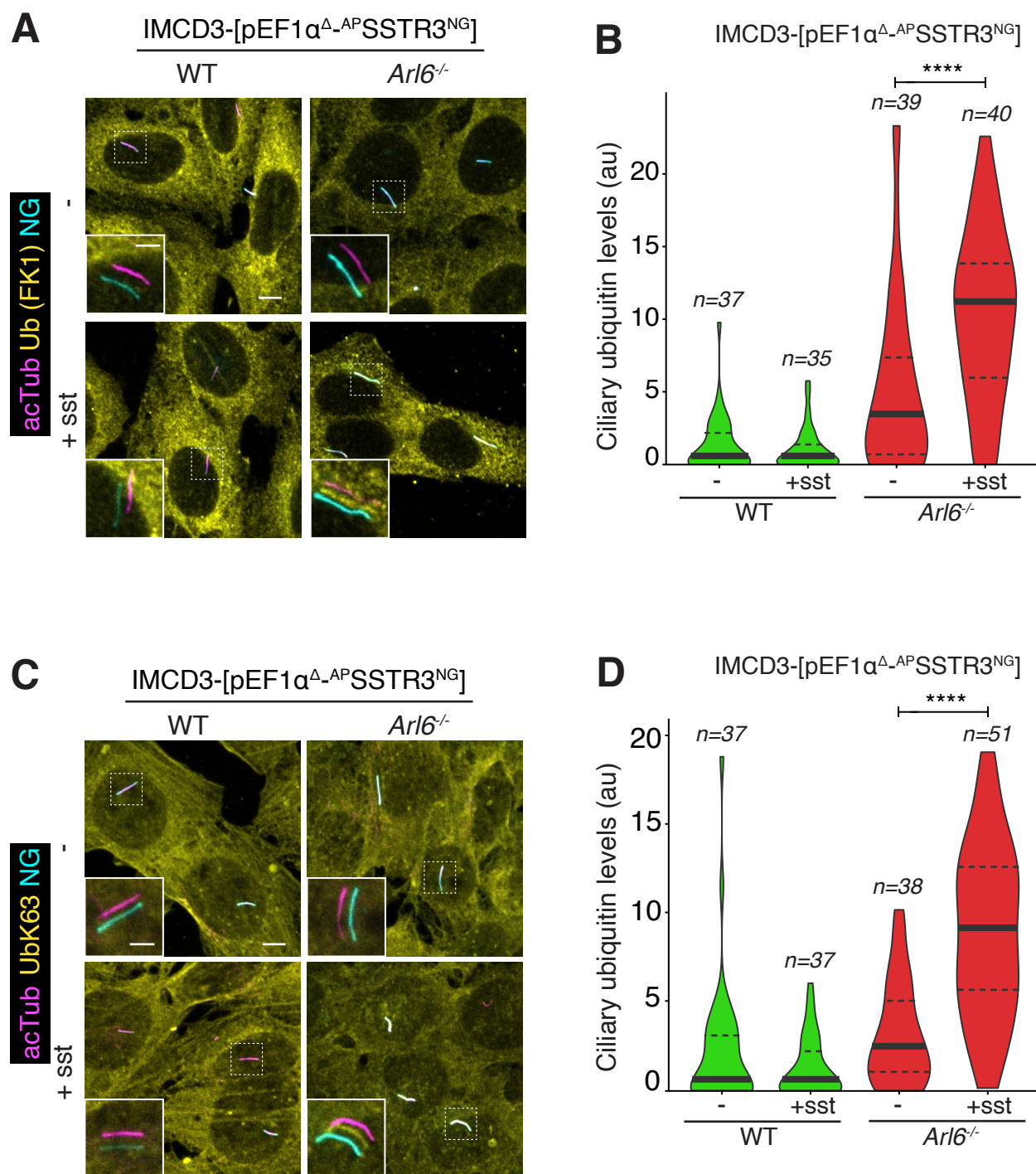
Figure 7

832 **Figure 7. Accumulation of ubiquitinated proteins in cilia of *Chlamydomonas* cells**

833 **and mammalian photoreceptors.**

834 **A.** *Chlamydomonas* cells of the indicated genotypes were fixed and stained for acetylated tubulin

835 (acTub, magenta) and ubiquitin (Ub, yellow). Scale bar: 5 µm. A weak ubiquitin signal detected

836 in WT cells is increased in *bbs4* mutant cells. **B.** Violin plots of the ciliary Ub levels in WT and

837 *bbs4 Chlamydomonas* cells. Asterisks indicate Mann-Whitney test significance values. ********, p=

838 <0.0001. The ciliary levels of Ub are increased more than 2-fold in *bbs4* cells as compared to

839 WT. **C.** Cilia purified from WT and *bbs4* cells via deciliation with dibucaine and differential

840 centrifugation were solubilized, and the protein contents resolved by SDS-PAGE. Immunoblots

841 for Ub (using the P4D1 antibody) and tubulin are shown. A rise in ubiquitin conjugates is

842 observed in *bbs4 Chlamydomonas* cells compared to WT. **D.** Mouse retina were fixed, embedded

843 and sectioned before staining for ubiquitin (Ub, yellow, lower panel), cone arrestin (magenta, a

844 marker of the photoreceptor outer segment layer) and DNA (cyan). OS: outer segment; IS: inner

845 segment; ONL: outer nuclear layer; OPL: outer plexiform layer; INL: inner nuclear layer. Scale

846 bar: 10µm. **E.** Model for the role of ubiquitin chains in selecting cargoes for signal-dependent

847 and constitutive exit via BBSome-mediated transport.

848

Supplementary Figure 1

849 **Figure S1. Signal-dependent ubiquitination of ciliary GPCRs**

850 **A.** IMCD3 cells of the indicated genotypes expressing ^{AP}SSTR3^{NG} were treated with

851 somatostatin (sst) for 2 h. Cells were fixed and stained for ubiquitin with the FK1 monoclonal

852 antibody (Ub (FK1), yellow) and acetylated tubulin (acTub, magenta). ^{AP}SSTR3^{NG} (cyan) was

853 imaged through the intrinsic fluorescence of NG. Channels are shifted in the insets to facilitate

854 visualization of overlapping ciliary signals. Scale bar: 5µm (main panel), 2µm (inset). **B.** Violin

855 plots of the fluorescence intensity of the Ub channel in the cilium in each condition are shown. A

856 3-fold increase in ciliary Ub signal is observed upon addition of sst to SSTR3-expressing cells.

857 Asterisks indicate ANOVA significance value. ********, $p = <0.0001$. **C.** IMCD3 cells of the

858 indicated genotypes expressing ^{AP}SSTR3^{NG} were treated with sst for 2 h. Cells were fixed and

859 stained for AcTub (magenta) and UbK63 (yellow). ^{AP}SSTR3^{NG} (cyan) was imaged through the

860 intrinsic fluorescence of NG. Channels are shifted in the insets to facilitate visualization of

861 overlapping ciliary signals. Scale bar 5µm (main panel), 2µm (inset). **D.** The fluorescence

862 intensity of the UbK63 channel in the cilium is represented as violin plots. Asterisks indicate

863 ANOVA significance value. ********, $p = <0.0001$.

Supplementary Figure 2

acTub DNA NPHP3^CTS

NPHP3^CTS - AMSH
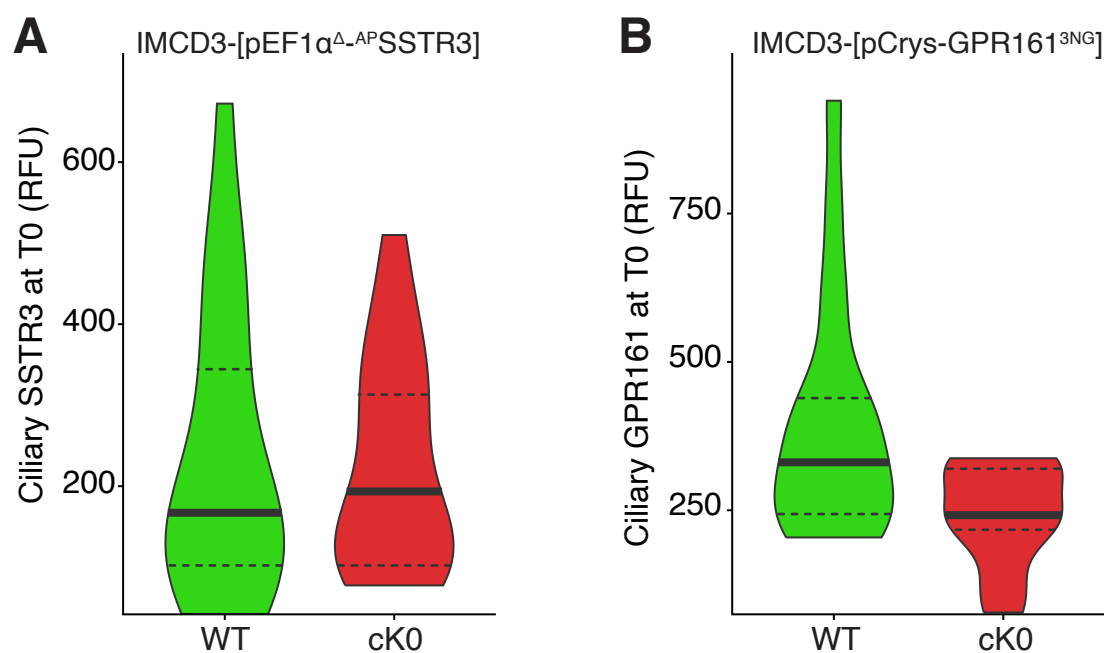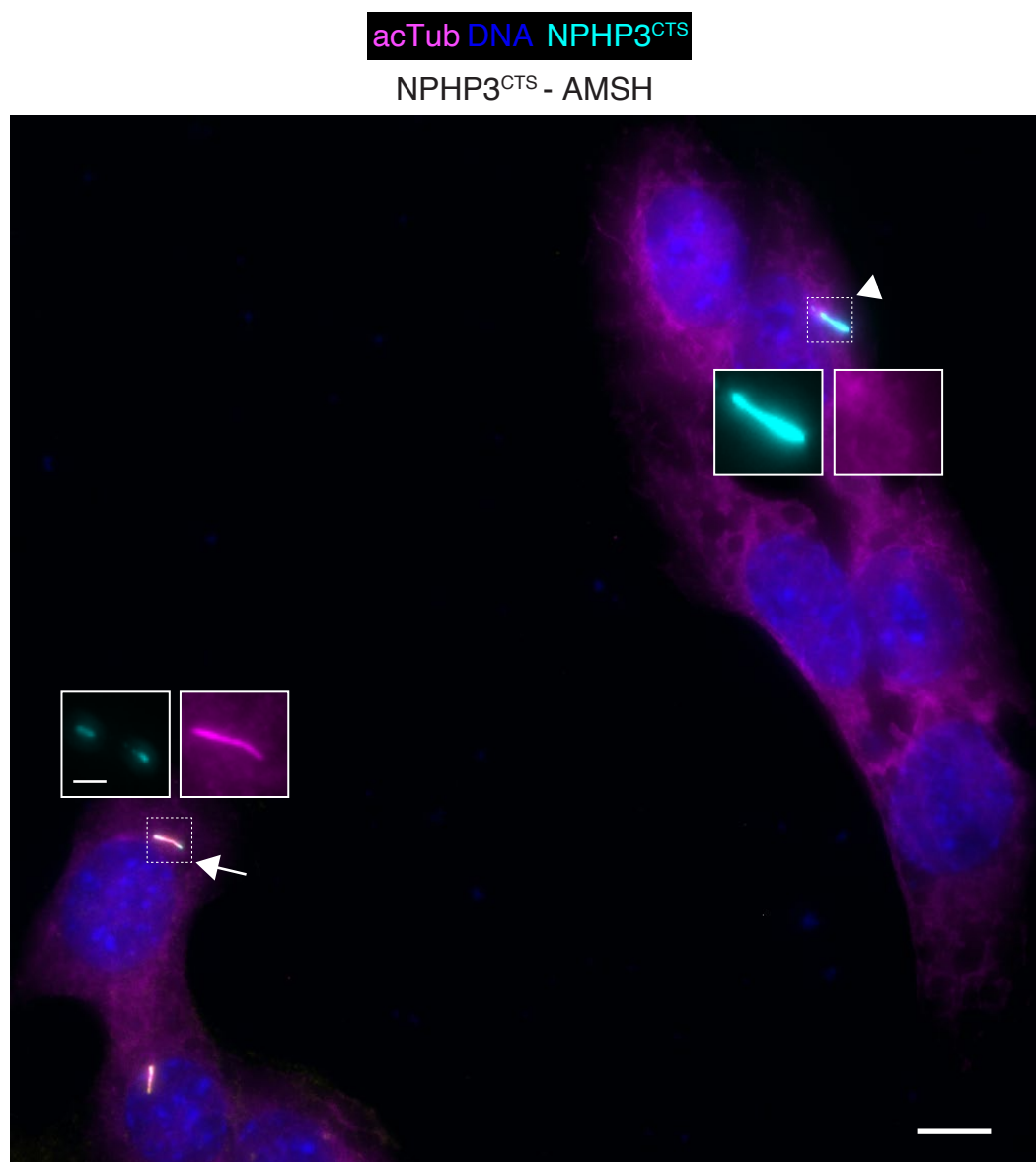
Supplementary figure 3
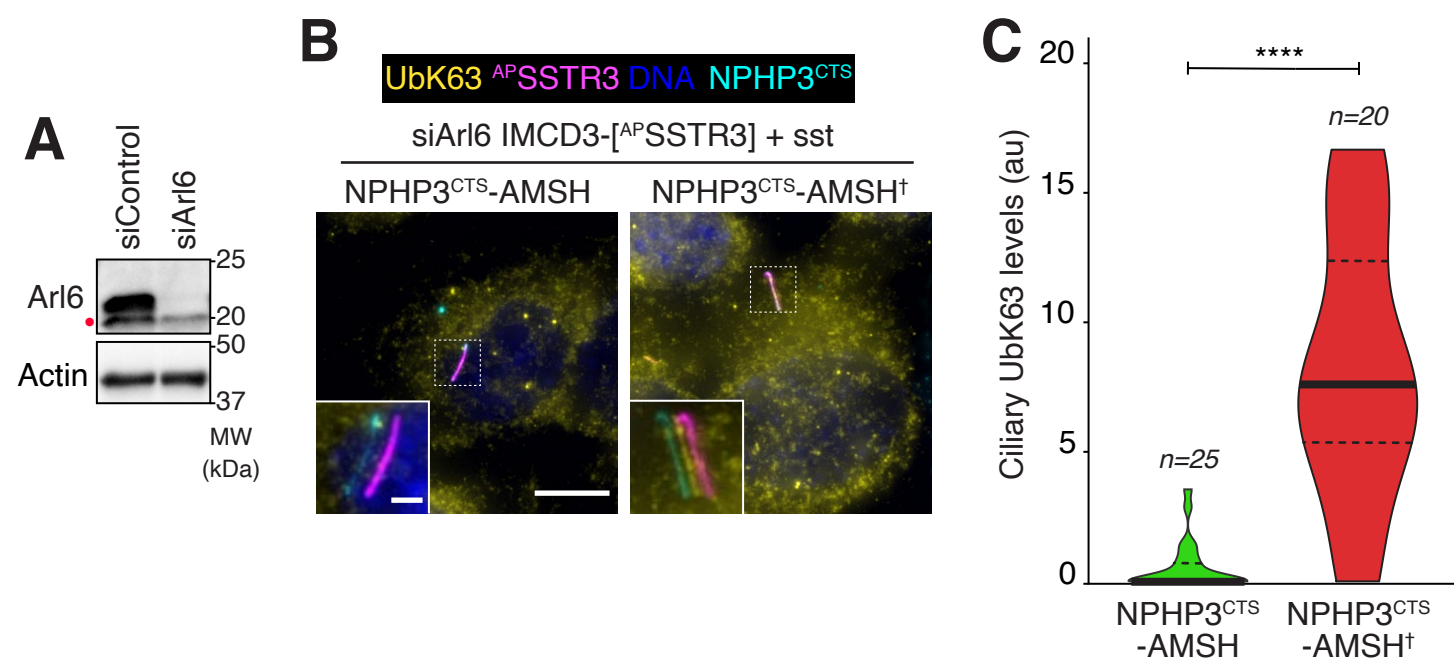
Supplementary figure 4

Figure S2. Fluorescence intensities of WT and cK0 GPCR variants at t=0.

A. Ciliary [AP]SSTR3 was pulse-labeled by addition of Alexa647-conjugated mSA (mSA647) to the medium for 5-10 min before addition of sst. Violin plots of the ciliary fluorescence intensities for WT and cK0 SSTR3 imaged in the far-red channel at t=0 are shown. **B.** Violin plots of the fluorescence intensities of NG fluorescence corresponding to WT and cK0 GPR161[NG] at t=0 are shown.

Figure S3. Expression levels of ciliary AMSH.

IMCD3-[pEF1α[Δ]-[AP]SSTR3; pEF1α-BirA•ER] cells were transfected with the plasmid expressing NPHP3[CTS]-AMSH as in Figure 4, before fixation and staining for acetylated tubulin (acTub, magenta) and DNA (blue). The NPHP3[CTS] fusions were visualized through the intrinsic fluorescence of GFP (cyan) A representative micrograph is shown. A cell expressing modest levels of cilia-AMSH is indicated by an arrow and possesses normal ciliary staining of acetylated tubulin. A cell expressing high levels of cilia-AMSH indicated by an arrowhead displays abnormal ciliary levels of acetylated tubulin. Cells with high ciliary levels of NPHP3[CTS]-AMSH were excluded from the analysis and only cells with modest ciliary levels of NPHP3[CTS]-AMSH were included in the experiment. Scale bar 5µm (main panel), 1µm (inset).

Figure S4. Cilia-targeted AMSH removes UbK63 chains from ciliary substrates.

A. IMCD3-[pEF1α[Δ]-[AP]SSTR3; pEF1α-BirA•ER] cells were transfected with control or Arl6 siRNAs. Cell lysates were immunoblotted for Arl6 or actin. A non-specific band cross-reacting with the anti-Arl6 antibody is marked with a dot. **B.** IMCD3-[[AP]SSTR3; BirA•ER] cells were transfected with siRNA targeting Arl6 and plasmids expressing NPHP3[CTS]-AMSH or NPHP3[CTS]- AMSH†. Surface-exposed [AP]SSTR3 was pulse-labeled with mSA647 for 5-10 min and cells were then treated with sst for 2h before fixation and staining for K63-linked ubiquitin chains (UbK63, yellow). The NPHP3[CTS]-AMSH fusions were visualized through the intrinsic fluorescence of GFP (cyan), [AP]SSTR3 was visualized via mSA647 (magenta) and DNA is blue.

38

891   Channels are shifted in the insets to facilitate visualization of overlapping ciliary signals. Scale bar

892   5µm (main panel), 2µm (inset). **C.** The fluorescence intensities of the UbK63 signal inside cilia

893   are represented as violin plots. Asterisks indicate Mann Whitney test significance value. ****, p=

894   <0.0001.

895

896

897

898 **MATERIALS AND METHODS**

899 **Cell culture**

900 The mouse IMCD3 cell lines used in the study were generated from a parental IMCD3-FlpIn

901 cell line (gift from P.K. Jackson, Stanford University, Stanford, CA). IMCD3-FlpIn cells were

902 cultured in DMEM/F12 (11330-057; Gibco) supplemented with 10% FBS (100-106; Gemini

903 Bio-products), 100 U/ml penicillin-streptomycin (400-109; Gemini Bio-products), and 2 mM L-

904 glutamine (400-106; Gemini Bio-products). The RPE1-hTERT cell line (ATCC CRL-4000) was

905 cultured in DMEM/F12 supplemented with 10% FBS, 100 U/ml penicillin-streptomycin, 2 mM

906 L-glutamine and 0.26% sodium bicarbonate (25080; Gibco).

907 Ciliation was induced by serum starvation in media containing 0.2% FBS for 16 to 24 h.

908

909 **Plasmid construction and Generation of stable cell lines**

910 Stable isogenic IMCD3 cell lines were generated using the Flp-In system (ThermoFisher

911 Scientific). Low-expression promoters and additional expression cassettes were introduced into

912 pEF5/FRT plasmid as described (Nager et al., 2017; Ye et al., 2018). To reduce expression

913 levels, the EF1α promoter was attenuated by mutating the TATA-box (pEF1α$^\Delta$) or replaced with

914 a minimal chicken lens δ-crystallin promoter (pCrys).

915 Coding sequences were amplified from plasmids encoding mouse GPR161 (BC028163;

916 Mammalian Gene Collection [MGC]; GE Healthcare), mouse SSTR3 (gift from Kirk Mykytyn,

917 Ohio State University, Columbus, OH), and human BBS5 (gifts from V. Sheffield, University of

918 Iowa, Iowa City, IA), BirA-ER (gift from Alice Ting). β-arrestin 2 (a gift from Mark Scott) was

919 stably expressed from a pCMV-based plasmid (pEGFP-N). SSTR3 and SMO expression were

920 driven by pEF1α$^\Delta$, GPR161 expression by pCrys, and BBS5 expression by pEF1α. Coding

921 sequences were fused to GFP, mNeonGreen (NG, (Shaner et al., 2013), or an acceptor peptide

922 for the biotin ligase BirA (AP) (Howarth and Ting, 2008). Multiple rounds of site-directed

923 mutagenesis were performed to generate SSTR3-cK0, a variant with all the cytoplasm-facing

40

924 lysine residues (K233, K330, K356, K407, and K421) mutated to arginine. GPR161-cK0, a

925 variant with 18 cytoplasm-exposed lysine residues (K83, K84, K93, K167, K247, K250, K269,

926 K296, K358, K362, K455, K469, K473, K481, K486, K497, K504, and K548) mutated to

927 arginine, was gene synthesized (GenScript). Cilia-AMSH was generated by fusing the catalytic

928 domain of mouse AMSH (gift from David Komander; Addgene plasmid #66712; (Michel et al.,

929 2015) with NPHP3(1-200) and GFP to create NPHP3[1-200]-GFP-AMSH[243-424]. A

930 catalytically dead version of AMSH was generated by mutating the water-activating Glu280

931 residue to Ala (Sato et al., 2008; Huang et al., 2013). pRK5-HA-Ubiquitin WT, K0 (all seven

932 acceptor lysine residues − K6, K11, K27, K29, K33, K48, and K63, are mutated to arginine) ,

933 and K63 only (all lysines except K63 mutated to arginines)(gift from Ted Dawson; Addgene

934 plasmid numbers − 17608, 17603, and 17606 respectively).

935 CRISPR-edited *Arl6⁻ᐟ⁻* and *Arl6⁻ᐟ⁻/Arrb2⁻ᐟ⁻* cell lines were described previously (Liew et al., 2014;

936 Nager et al., 2017). The genotypes are *Arl6*, NM_001347244.1:c.- 10_25del; c.3_6del; and *Arrb2*,

937 NM_001271358.1:c.1 12del;c112_113del.

938

Transfection

940 For generation of all stable cell lines except for the ones expressing β-arrestin 2^{GFP}, FRT-based

941 plasmids were reverse transfected using XtremeGene9 (Roche) into IMCD3 Flp-In cells along

942 with a plasmid encoding the Flp recombinase (pOG44) and stable transformants were selected by

943 blasticidin resistance (4 μg/ml). The transfection mixture was then added to the cells. pEGFP-N•

944 β-arrestin 2-GFP was transfected into IMCD3 cells using Lipofectamine 2000, and clones were

945 selected using neomycin resistance.

946

Antibodies and drug treatments

948 The following monoclonal antibodies were used for immunofluorescence: anti-acetylated tubulin

949 (mouse; clone 6-11B-1; Sigma-Aldrich; 1:500), anti-ubiquitin clone FK2 was used in all

950   experiments except where indicated (mouse; D058-3; Medical and Biological Laboratories;

951   1:500), anti-ubiquitin FK1 in **Fig. S1A-B** (mouse; D071-3; Medical and Biological Laboratories;

952   1:500), anti-ubiquitin K48 linkage (rabbit; clone Apu2; 05-1307; Millipore-Genentech; 1:500),

953   anti-ubiquitin K63 linkage (human; clone Apu3; a gift from Genentech; 1:500). The following

954   monoclonal antibodies were used for immunoblotting: anti-ubiquitin (mouse; clone P4D1; 3936;

955   Cell Signaling; 1:1000), anti-α tubulin (mouse; clone DM1A; MS-581-P1ABX; Thermo

956   Scientific;1:1000), anti-HA (mouse; clone 16B12; 901501; Biolegend;1:500), streptavidin-HRP

957   (Pierce-21140;Thermo Scientific; 1:10000). The following polyclonal antibodies were used for

958   immunofluorescence: anti-GPR161 (rabbit; 13398-1-AP; Proteintech; 1:100), anti-Smoothened

959   (rabbit; a gift from Kathryn Anderson, Memorial Sloan Kettering Cancer Center, New York,

960   NY; 1:500), anti-cone-arrestin (rabbit; AB15282; Millipore; 1:500). Biotinylated SSTR3 and

961   GPR161 were detected using Alexa Fluor 647–labeled monovalent streptavidin (mSA647) (Ye et

962   al., 2018). The following reagents were used at the indicated concentrations: 200 nM SAG and

963   10 µM somatostatin 14. Somatostatin 14 stocks were made in DMEM/F12 media, HEPES, no

964   phenol red (11039-021, GIBCO). SAG was dissolved in DMSO (276855, Sigma-Aldrich).

965

Imaging and microscopy

967   Cells were imaged either on a DeltaVision system (Applied Precision) equipped with a PlanApo

968   60x/1.40 objective lens (Olympus), CoolSNAP HQ2 camera (Photometrics), and solid-state

969   illumination module (InsightSSI), or on a confocal LSM 700 (Zeiss) microscope equipped with

970   40x Plan-Apochromat 1.3 DIC oil objective. Z stacks were acquired at 0.5 µm interval (LSM

971   700, Figs. 1, 3, 7, and S1) or 0.2 µm interval (DeltaVision, Figs. 4, 6, S3, and S4).

972   For fixed imaging, 60,000 cells were seeded on acid-washed coverglass (12 mm #1.5; 12-545-81;

973   Thermo Fisher Scientific). Cells were grown for 24 h and then starved for 16-24 h in 0.2% FBS

974   media before experimental treatment. After treatment, cells were fixed with 4%

975   paraformaldehyde in PBS for 15 min at 37°C and extracted in -20°C methanol for 5 min. Cells

976   were then permeabilized in IF buffer (PBS supplemented with 0.1% Triton X-100, 5% normal

977   donkey serum (017-000-121; Jackson ImmunoResearch Laboratories), and 3% bovine serum

978   albumin (BP1605-100; Thermo Fisher Scientific)), incubated at room temperature for 1h with

979   primary antibodies diluted in IF buffer, washed three times in IF buffer, incubated with

980   secondary antibodies (Jackson ImmunoResearch Laboratories) diluted in IF buffer for 30 min,

981   and washed three times with IF buffer. DNA was stained with Hoechst 33258 (H1398; Molecular

982   Probes), cells were washed twice more with PBS, and coverglass mounted on slides using

983   fluoromount-G (17984-25; Electron Microscopy Sciences).

984   For live-cell imaging, 300,000 cells were seeded on acid-washed 25mm cover glass (Electron

985   Microscopy Sciences). After 24 h of growth, cells were serum starved for 16 h and transferred to

986   the DeltaVision stage for imaging at 37°C within an environmental chamber that encloses the

987   microscope and the stage. Cells were imaged in DMEM/F12 media, HEPES, no phenol red

988   (11039-021, GIBCO). To measure SSTR3 exit, cells expressing ^{AP}SSTR3 were first washed three

989   times with PBS and then pulse-labeled with 2μg/ml mSA647 for 5 min at 37°C. Cells were then

990   imaged after addition of sst (for SSTR3) or SAG (for GPR161) for 2 h with an acquisition every

991   10 min. Each acquisition consisted of a 3-plane Z-stack with each plane separated by 0.5 μm.

992   Transmittance was set to 5% and exposure time to 500 ms.

993   WT or *Bbs4$^{-/-}$* mice (Mykytyn et al., 2004) eyes were enucleated at P21. Whole eyes were fixed in

994   4% paraformaldehyde/PBS overnight at 4°C and then washed three times with PBS. The eyes

995   were infiltrated in 30% sucrose/PBS at 4 °C overnight. Eyes were placed in OCT compound

996   embedding medium (4583; Tissue-Tek), frozen on dry ice, and stored at −80 °C. 14 μm sections

997   were cut on a cryostat (CM 1850; Leica). Sections were processed for immunofluorescence as

998   follows. Sections were blocked in blocking solution (50 mM Tris pH7.4, 100 mM NaCl, 0.1%

999   Triton-X 100, 3% normal donkey serum, and 0.1% BSA) for 1 h at room temperature, then

1000   incubated with primary antibodies overnight at 4°C, followed by three washes in wash solution

1001   (50 mM Tris pH7.4, 100 mM NaCl, and 0.1% TX100). After rinsing in wash solution, sections

1002   were incubated with secondary antibodies for 1 h at room temperature. DNA was counterstained

1003   using Hoechst 33258 dye, sections washed twice more with PBS, and mounted on slides using

1004   Fluoromount-G. Sections were imaged on Confocal LSM 700 (Zeiss) microscope.

1005

1006 **Image analysis**

1007 Files were imported from the Deltavision or LSM700 workstations into ImageJ/ Fiji (National

1008 Institutes of Health) for analysis. For the quantification of ciliary ubiquitin signal in fixed cells,

1009 maximum intensity projections were used. The ciliary ubiquitin intensity was measured using the

1010 following equation:

1011 $F_{Ub\text{-}cilia} = F_{Ub\text{-}cilia\_measured} - F_{background}$

1012 $F_{Ub\text{-}cilia\_measured}$ is the total ciliary ubiquitin fluorescence detected, $F_{background}$ is the background

1013 ubiquitin fluorescence measured in the adjacent area. For all measurements, the fluorescence

1014 integrated density was used. $F_{Ub\text{-}cilia}$ were plotted as violin plots using the PlotsOfData web tool

1015 (https://huygens.science.uva.nl/PlotsOfData/). Each violin represents the distribution of data,

1016 which includes all the data points. Median and interquartile range is marked by solid and dotted

1017 lines, respectively. No gamma adjustment was applied during figure preparation; all the

1018 representative micrographs for respective panels are displayed within the same dynamic range.

1019 For some representative micrographs, the most in-focus plane was used rather than the

1020 maximum intensity projection (Fig.3, and Fig. 6, panel A and C).

1021 To measure SSTR3 exit, the integrated density of Alexa Fluor 647 fluorescence in the maximum

1022 intensity projection was measured for each time point. The cilia-adjacent fluorescence was

1023 subtracted as the background, and a mathematical photobleaching correction was applied:

1024 $F_{cilia} = (F_{mSA647\_measured}/F_{mSA647\_1}) + ((1 - e^{-\lambda}) * (n - 1))$, where λ is the photobleaching decay

1025 constant, n is the number of images taken, $F_{mSA647\_measured}$ is the integrated mSA647 fluorescence

1026 measured for image n, F_{mSA657_1} is the measurement for the first time point, and F_{cilia} is the

1027 reported fluorescence. In this equation, F_{cilia} is reported in relative fluorescence units (RFUs).

1028 [AP]GPR161[3NG] exit was followed similarly with the difference that NG fluorescence intensity was

1029 measured. For SSTR3 as well as GPR161, photobleaching corrected data (F_{cilia}) for each

1030 condition were linearly fitted ($F_{cilia} = m * time + c$) and plotted in Excel.

1031   Endocytosed SSTR3 foci were revealed by contrast enhancement and counted with the ImageJ

1032   particle analysis tool.

Chlamydomonas culture, isolation of flagella and immunofluorescence

1034   *Chlamydomonas* WT- g1 (nit1, agg1, mt+) [gift from George B. Witman, University of

1035   Massachusetts Medical School, Worcester, Massachusetts]and *Bbs4*- CC-4377 ptx5-1/bbs4-1::

1036   NIT1 agg1 mt+ (Chlamydomonas Resource Center) strains were cultured asynchronously under

1037   light in TAP media (Gorman and Levine, 1965) for 72 h. Flagellar fractions were prepared from

1038   two liters of cultures of WT or *Bbs4* cells as described (Craige et al., 2013). Briefly, cells were

1039   harvested by centrifugation for 5 min at 2,000 rpm (1,100 x g) at room temperature. Cells were

1040   resuspended in 10 mM HEPES, pH 7.4 and centrifuged for 5 min at 2,000 rpm (1,100 x g). Next,

1041   the cell pellet was gently resuspended in ice-cold HMDS (10 mM HEPES, pH 7.4, 5 mM

1042 $MgSO_4$, 1 mM DTT, and 4% (w/v) sucrose). Deflagellattion was achieved by addition of 5 mM

1043   dibucaine to each tube of cells and by pipetting up and down ~10 times using a 10-ml plastic

1044   serological pipette. The suspension was spun for 5 min at 1,800 x g at 4°C. The supernatant

1045   containing flagella was underlaid with 9 ml ice-cold HMDS-25% sucrose (10 mM HEPES, pH

1046   7.4, 5 mM $MgSO_4$,1 mM DTT, and 25% (w/v) sucrose), followed by a centrifugation step for 10

1047   min at 2,800 rpm (2,400 x g), 4°C. The supernatant above the sucrose interface was collected

1048   using a 25-ml serological pipette and flagella were pelleted by centrifugation for 20 min at 30,000

1049   x g (16,000 rpm), 4°C. The flagellar pellet was resuspended in 100 µl HMDS buffer. Protein

1050   concentrations were measured by Bradford and 25 ug were resolved by SDS-PAGE for

1051   immunoblotting.

1052   *Chlamydomonas* immunofluorescence was performed as follows. Cells were fixed with 4 %

1053   paraformaldehyde in MT buffer* (30 mM HEPES, pH7, 5 mM EGTA, 5 mM MgSO4, and

1054   25mM KCl) for 20 minutes in suspension. The cells were centrifuged at 1000 rpm for 5 minutes,

1055   resuspended in 100 µl of fixative and transferred onto slides coated with 1 mg/ml poly-L-lysine.

1056   After 5 minutes, the unadhered cells were washed off by rinsing with PBS. Cells were

1057   permeabilized in 0.5% Triton-X 100 for 20 minutes followed by blocking for 1 h in blocking

1058   buffer (3% fish skin gelatin, 1% BSA, 0.1% Tween20 in PBS) at room temperature. Cells were

1059   incubated at 4°C overnight with primary antibodies diluted in blocking buffer, washed five times

1060   in PBS and incubated with secondary antibodies for 2 h at room temperature. After five washes

1061   in PBS, coverglasses were mounting on slides using Fluoromount-G. Cells were imaged on the

1062   LSM700 confocal microscope.

1063

1064   **Biochemical analysis of SSTR3 ubiquitination**

1065   IMCD3 cells stably expressing pEF1α$^{\Delta\text{-AP}}$SSTR3^{NG} and BirA-ER were transiently transfected

1066   with HA-tagged ubiquitin plasmids. Cells were reverse transfected using XtremeGene9 and

1067   plated into 15 cm plates. Cells were moved to medium containing 0.2% serum and

1068   supplemented with 10 μM biotin 24 h after transfection to promote ciliation and maximize

1069   biotinylation of SSTR3. 18h after the medium change, sst was added for 0, 10 or 20 min. The

1070   assay was stopped by washing cells twice with ice-cold 1xPBS and scraping cells off on ice into

1071   1ml of ice-cold RIPA buffer (50 mM Tris/HCl pH 8, 150 mM NaCl, 1% Nonidet P-40, 0.5%

1072   sodium deoxycholate, 0.1% SDS, 100 mM iodoacetamide, 10mM EDTA) supplemented with

1073   protease inhibitors (1 mM AEBSF, 0.8 mM Aprotinin, 15 mM E-64, 10 mg/mL Bestatin, 10

1074   mg/mL Pepstatin A and 10 mg/mL Leupeptin). After gently rocking at 4°C for 5 minutes,

1075   lysates were clarified by spinning in a tabletop Eppendorf centrifuge at 15,000 rpm and 4°C for

1076   20 minutes. Each clarified lysate was incubated with 50μl of streptavidin Sepharose beads (GE

1077   Healthcare) for 1 h at 4°C to capture biotinylated SSTR3. Beads were washed four times with

1078   500μl of RIPA buffer and bound proteins were eluted by heating the beads in 1X LDS sample

1079   loading buffer containing 2 mM biotin at 70°C for 10 minutes. After SDS-PAGE and transfer,

1080   PVDF membranes were probed with anti-HA antibody and streptavidin-HRP.

1081   Signals were acquired with a ChemiDoc imager (Bio-Rad) and analyzed with ImageLab 6.0.1

1082   (Bio-Rad). The integrated densities of the SSTR3 bands in the streptavidin-HRP blot were

1083   normalized to the integrated densities of the endogenous biotinylated proteins to correct for

1084   variations in the recovery of biotinylated proteins on streptavidin Sepharose. The resulting value

1085   is SSTR3$_{bio}$. Second, the integrated densities of ubiquitinated SSTR3 were collected by

1086   measuring the area from 100 kDa to the top of the gel on the HA blot. The values were

1087   background-corrected by subtracting the value of the equivalent area in the IMCD3 control lane.

1088   The resulting value is Ub-SSTR3$_{raw}$. The relative amount of SSTR3 that is ubiquitinated, Ub-

1089   SSTR3$_{frac}$ = Ub-SSTR3$_{raw}$/SSTR3$_{bio}$ was plotted on the graphs using PlotsOfData (Postma and

1090   Goedhart, 2019).

1091